AD NUMBER

AD862773

LIMITATION CHANGES

TO:

Approved for public release; distribution is unlimited.

FROM:

**Distribution authorized to U.S. Gov't. agencies and their contractors;
Administrative/Operational Use; FEB 1969. Other requests shall be referred to Air Force Armament Lab., Eglin AFB, FL 32542.**

AUTHORITY

AFATL ltr 14 Sep 1976

AFATL-TR-69-14

AD 862773

EFFECTS OF FILLER MATERIAL ON BOMB FRACTURE

M. H. MILLER
R. W. JOHNSON
AVCO GOVERNMENT PRODUCTS GROUP
SPACE SYSTEMS DIVISION

TECHNICAL REPORT AFATL-TR-69-14

FEBRUARY 1969

This document is subject to special export controls and each transmittal to foreign governments or foreign nationals may be made only with prior approval of the Air Force Armament Laboratory (ATRW), Eglin AFB, Florida 32542.

AIR FORCE ARMAMENT LABORATORY
AIR FORCE SYSTEMS COMMAND • UNITED STATES AIR FORCE
EGLIN AIR FORCE BASE, FLORIDA

71

EFFECTS OF FILLER MATERIAL ON BOMB FRACTURE

M. H. Miller
R. W. Johnson

FOREWORD

This report was prepared by Avco Government Products Group, Space Systems Division, Lowell, Massachusetts, under Contract Number F08635-68-C-0129 for the Air Force Armament Laboratory, Eglin Air Force Base, Florida. This analytical study was performed during the period 13 June 1968 to 12 January 1969. Lt. John H. Bennett (ATRW) monitored the program for the Armament Laboratory.

The Program Manager was M. H. Miller, and R. W. Johnson served as Project Engineer.

Contributions to this study were made by Mr. D. Oplinger, who provided theoretical background and interpretation of results, Mr. E. Lawlor and Dr. J. McElman, who consulted on various aspects of the study, and Miss C. Christie who worked with the computer runs and output.

Information in this report is embargoed under the Department of State International Traffic in Arms Regulations. This report may be released to foreign governments by departments or agencies of the U. S. Government subject to approval of the Air Force Armament Laboratory (ATRW), Eglin AFB, Florida 32542, or higher authority within the Department of the Air Force. Private individuals or firms require a Department of State export license.

This technical report has been reviewed and is approved.

Charles K. Arpke, Lt. Colonel, USAF
Acting Chief, Technology Division

ABSTRACT

Avco Corporation, Space Systems Division, has completed a six month analytical program which investigated the effects of the explosive filler material on the structural failure of bomb casings during impact and penetration into hard targets.

A typical cylindrical shell, similar to the present BLU-31B bomb, was studied. Both constant and linearly varying wall thicknesses were investigated. To obtain a basic understanding of the filler effect, only an axial load, suddenly applied and held constant, was included. A finite element solution was used to obtain resulting stresses and displacements within the casing. Results indicate the large effect of the filler on the hoop stresses. These stresses are of sufficient magnitude to induce casing failure based on current bomb designs and impacting conditions against concrete targets.

Results are presented for a typical Composition B explosive filler materiel. Hoop stress magnitudes may be obtained for any other filler material, using given relationships between its bulk modulus and density properties compared to the Composition B properties.

(The reverse of this page is blank)

TABLE OF CONTENTS

LIST OF FIGURES

LIST OF FIGURES (Concl'd)

LIST OF TABLES

SECTION I

INTRODUCTION

In recent years there has been increased interest in the feasibility of burying an explosive-carrying bomb deep within a target before detonation. The United States Air Force, Navy, and Army, as well as other government agencies, are actively investigating the problems associated with this concept of target defeat mechanism. Types of targets range from railroad beds, airplane runways, roads, dams, bunkers, pillboxes, piers, gun emplacements and structural foundations. These targets are constructed of a variety of materials: earth, sand, gravel, logs, concrete, or rock.

A bomb encountering a concrete target will experience loads much greater than if it attacked an earth target. To remain structurally intact and still not explode during the impact and subsequent penetration of the target, the bomb structure must be able to withstand the high stresses imposed without failure of the bomb structural components. A simple approach is to design a massive structure which will not fail under any circumstances. This approach, however, usually entails a large sacrifice of explosive capability. A better approach is to attempt to understand the causes of bomb failure and to then formulate loading criteria and develop a rational bomb design to achieve maximum explosive capability while maintaining structural integrity. Because of the wide range of loadings expected from encountering extremes of target materials, it may be appropriate to have a family of bomb designs to optimize the available volume allotted for explosive filler, according to classes of targets.

An alternative approach is to attempt to establish the bounds on the target spectrum for any particular bomb. One such weapon is the Air Force BLU-31B bomb which has been used for the attack of earth-type targets. This bomb is essentially flat-ended on its impact end. Recently, it was decided to investigate the possibility of using this bomb against concrete targets. Therefore, a test program was undertaken in which BLU-31B bombs were impacted against concrete targets. Bomb case failures were experienced in the form of large, long cracks in the longitudinal direction indicating hoop stresses in excess of allowables. The explosive filler was present in these tests and no detonations occurred. It was suggested that the filler may have contributed to the failure of the bomb cases.

The analytic work presented in this report is an outgrowth of these tests. It was the goal of this analytic program to provide a basic understanding of the effect of the filler material on the structural integrity of a bomb under impact conditions into hard targets. Although the approach used was not overly sophisticated, and several simplifying assumptions have been made, results obtained will provide the basis for understanding the role which the filler plays in the total shell loading picture.

SECTION II

SUMMARY

A 6-month analytic study has been performed to investigate the effects of the filler material on the structural failure of bomb casings resulting from impact into hard targets. The contribution of the stresses caused by the filler during this impact and penetration event has been determined. To develop a basic understanding of the importance of the filler material, a simplified bomb structure was analyzed, with a fundamental, axial load only, impact condition.

Only a blunt-ended configuration was considered. Two types of shell designs were inspected: one with uniform thickness, and one with a linearly-varying thickness. The configurations chosen resembled the present day BLU-31B design in length, diameter, and shell wall thickness.

The filler material was idealized as a fluid whose only interaction with the shell casing was as a radial pressure acting on the shell walls. The effects of bonding between the filler and the shell were ignored.

A finite element solution to this problem was formulated and solved, using existing computer programs at Avco/SSD. The forcing function used was a step axial force which, in addition to acting axially on one end of the shell, induced axial and corresponding radial pressure waves in the filler material which traversed the length of the cylinders.

Results indicate that for the idealized models considered, the filler contributes negligibly to the axial stresses in the shell. However, the filler induces hoop tensile stresses which are of such high magnitude that they can cause failure of a bomb casing. This failure is in the form of longitudinal splitting apart of the shell. The presence of stress-concentration-producing welded joints or plugs would be especially vulnerable to this type of stress failure. These tensile hoop stresses can be as large as 162,000 psi for a BLU-31B class bomb impacting at 1000 ft/sec. Such a stress would develop near the rear end of the shell during a head-on impact of the blunt-ended bomb with a concrete target.

The hoop stresses computed in this report are for a typical Comp B explosive filler and may be considered as a baseline reference. Hoop stress magnitudes may be found for any filler material, knowing its bulk modulus and density properties, and comparing relationships involving these properties with the baseline analysis. It is thus possible to estimate filler effects for any filler material.

The results of this study have pointed out areas requiring more detailed investigation. These include the study of the bonding between the filler material and the shell wall. The axial and radial restraint which this bonding would impose upon the system should reduce the shell stresses, but will complicate the stress patterns in the filler material itself. Effects of filler damping properties could also alter the total stress situation in the shell.

Another area of importance is the magnitude and shape of the forcing function acting on the shell. This has an extreme effect on stresses felt near the rear end of the shell and can significantly affect the design of the bomb. Only an axial step force, applied instantaneously and held constant, was considered in

this study. The typical penetrating bomb design utilizes a conical or ogival nose shape design. With such a configuration, the forcing function is not a step function, but rather a force which increases with time, peaks, and then decays relatively slowly with time. Hoop stresses for this type of configuration could be drastically different from those found in this study.

SECTION III

TECHNICAL APPROACH AND METHOD OF ANALYSIS

A present requirement for certain bomb and projectile designs is the capability to penetrate a target before detonation of the explosive filler. The resulting underground burst has significant advantages over a surface burst for many military applications. To accomplish this requirement, the projectile must remain structurally intact during the impact and penetration events. Typical targets include sand, gravel, soils, concrete, and rock. Extremely high resisting forces are encountered during this process, which may result in structural failure, or premature detonation of the explosive by excessive stresses or deformations.

To overcome structural failure or excessive deformations, the shell walls of the projectile must be capable of withstanding the penetration loads, preferably without permanent deformation, i.e., the shell wall should not be stressed beyond its elastic limit. Stresses in the wall are caused by the inertial reactions of both the projectile structure and the explosive filler.

The magnitude of these stresses depends on many factors, such as: angle of impact, impact velocity, nose geometry, explosive cavity geometry, explosive material properties, projectile mass distribution, and target material properties.

The present investigation studies the effect of the filler material on shell stresses under axial loading conditions. This type of loading occurs during a head-on impact with the target in which it is assumed that no lateral bending motions are induced. This normal impact case although relevent, is a highly simplified example. Generally, the impact will be at some oblique angle to the target surface. Resisting forces for the general case are composed of axial and lateral components which set up axial and lateral translational decelerations, and rotational decelerations as well. Therefore, the total loading configuration is highly complex. To obtain a basic understanding of the effect of the filler material, only the axial component will be considered in this report. This will eliminate variables associated with lateral motions. Also, since this is the actual loading condition in normal impacts, it is thus a logical starting point for any study of this type. Only as the impact angle changes from the normal do the other loadings become increasingly important.

The stresses in the projectile under this axial loading condition will be found by a finite element approach, where the structural system is idealized by an analytical model which simulates the actual structure. The stresses of interest are in the walls of the projectile shell. Since failure is assumed to take place when plastic deformation of the shell occurs, only the elastic solution to the problem of shell response is considered. This happens when the yield strength of the shell material is reached.

The solution to this problem is obtained through the use of the finite element routines presently available at Avco. These programs, the 1384 and the 1520 computer codes, solve for the transient response of systems subjected to arbitrary time-varying forces. Program 1384 treats linear elastic systems. Program 1520 handles, in addition, forcing functions which are dependent upon local system displacements and velocities as well as the time domain. In general, the codes solve the matrix set of equations:

$$M\ddot{x}_i + C\dot{x}_i + Kx_i = F_i \qquad (1)$$

where

M = inertia matrix

C = damping matrix

K = stiffness matrix

F = forcing functions

x_i = coordinates of the finite element system, at the ith location.

The bomb under consideration will be a circular cylindrical shell of variable thickness, with a front and back plate attached at each end of the cylinder, and the filler material within the cavity. Thus, the shell has given boundary conditions at its ends. The initial stress wave is axially induced as a step input at the front end plate. The analysis does not pertain to wave action within the end plates, but is concerned only with the response in the cylindrical shell itself. Both axial and radial motions of the shell are considered. The filler material is assumed to act essentially independent of the shell structure, with no axial interaction with the walls.

In the finite element model, only the shell structure is considered, with its own mass and stiffness properties. The filler enters the analysis as a forcing function which is a radial pressure wave traveling axially up and down the length of the shell. The axial compression induced in the filler by the impact will cause the radial pressure exerting on the shell walls. The magnitude of this pressure is time-dependent, and is a function of the axial resisting force acting on the projectile as a whole. No shear effects or radial restraints, transferred by the bonding material between the shell and the filler, are considered.

End effects depend greatly on the nose shape and filler cavity geometry at the front end, and upon the base plug and shell wall thicknesses at the rear end. For this analysis the model consists of a circular cylindrical shell of variable thickness. The end conditions are treated as restraints at the two ends. At these points, no radial displacement (w) or rotation (β) is allowed. This restrains the ends from expanding radially or rotating, which is what nose and base caps would accomplish.

The finite element system is composed of a series of nodal circles. Each nodal circle describes the motion of the idealized system at that given location. Thus, each nodal circle has coordinates (x) associated with it. The coordinate system, shown in Figure 1, is composed of axial (u), tangential (v), radial (w), and bending (β) components. For the pure axial loading conditions being considered, the tangential (v) component is eliminated, since no torsion exists. The bending coordinate (β) still remains, however, since it describes shell motion resulting from different radial displacements at successive locations along the axis of the body.

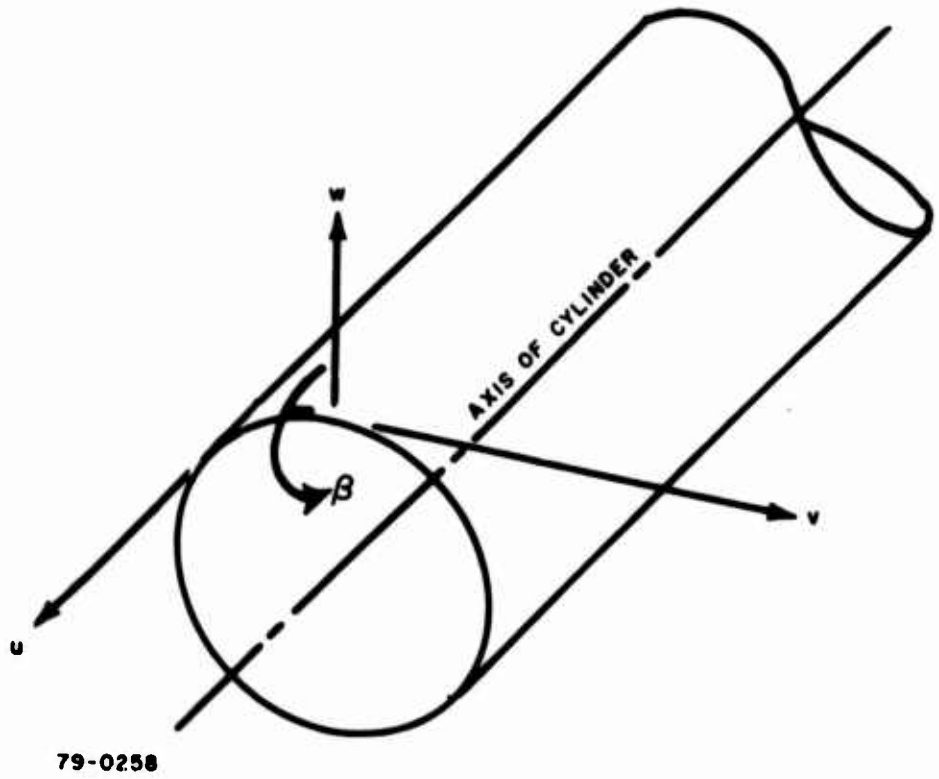

Figure 1 Displacements Considered at Each Nodal Circle

The mass and stiffness matrices are obtained by using Avco Computer Program 2222. This shell static analysis program was orginally developed at the Massachusetts Institute of Technology and is described in Reference 1. Basically, it solves for static stresses and displacements of a body of revolution to an arbitrary forcing function. A by-product of the analysis is the generation of the mass and stiffness matrices of the system under consideration.

Both the M and K matrices in general exhibit coupling between the μ, ν, w, and β motions. For pure axial force excitation, no tangential forces or displacements arise, and the displacements are independent of the location along the circumference of the shell at a given node. If the forcing function and resulting displacements and stresses are expressed in terms of a Fourier series, the pure axial case is completely described by the zero harmonic ($n = 0$), based on the general expression $\cos n\theta$ for variation with circumferential location. In the case of a lateral load, the first harmonic ($n = 1$) and perhaps higher harmonics may be required to adequately express lateral motions. It should be noted that the capability to handle lateral forcing functions exists in the present model formulation.

The shell under consideration in this study has a blunt front end. As such, it will experience suddenly applied forces upon impact. The magnitude of this force will depend upon the properties of the target material. For the targets assumed in this study, failure of the target will occur and the blunt-ended projectile will penetrate into the target. The target will continually resist this penetra-

tion until the projectile comes to rest or perforates the target. For a number of years Avco has been analytically and experimentally investigating the forces resisting penetration of a hard target by a projectile (References 2, 3, and 4). These forces are highly transient in nature, rising to a peak value in fractions of a millisecond, and then decaying relatively slowly during the remainder of the penetration event. Typical axial resisting forcing functions for a normal impact (at 90 degrees to the target surface) are shown in Figure 2 for two typical projectiles.

This figure illustrates the dependency of the force-time relation on the nose shape of the projectile and the variation of the resisting force with time as penetration progresses. Test results have shown the peak strains to occur well before the nose section has completely entered the target.

To assess the effects of the filler in this present study, the forcing function is assumed to be a step axial force, which remains constant throughout the time of interest. Since this is a linear elastic analysis, resulting stresses and displacements are linear with the force magnitude, and may be ratioed directly for any change in amplitude of the forcing function.

For this analysis, the magnitude of the axial force is determined by the resistance expected during penetration of a concrete target. As mentioned earlier, Avco has developed a basic penetration force law to predict loads encountered during an impact and penetration event. This force, based on Poncelet's form for the force resisting motion through a hard medium, is proportional to a material constant plus a term dependent on the square of the projectile velocity during penetration. Empirical constants have been formulated for various target media from analysis of experimental data over the past several years. Effects of target and projectile properties are included in the basic equation, which has the form:

$$F = A\left(\eta + \frac{1}{2}\rho\ C_d V^2\right)$$

where

F = resisting force

A = cross-sectional area of projectile in a contact with the target

η = target bearing strength factor

ρ = target density

C_d = drag coefficient of projectile

V = penetrator velocity

The capability of the finite element approach to adequately predict stress wave propagation in certain types of problems has been demonstrated in Reference 5. In that report, free-free and fixed-free uniform rods were impacted longitudinally by a given mass. Resultant stresses throughout the bar were computed by classical theory (Timoshenko, Reference 6, and Love, Reference 7) and compared with the

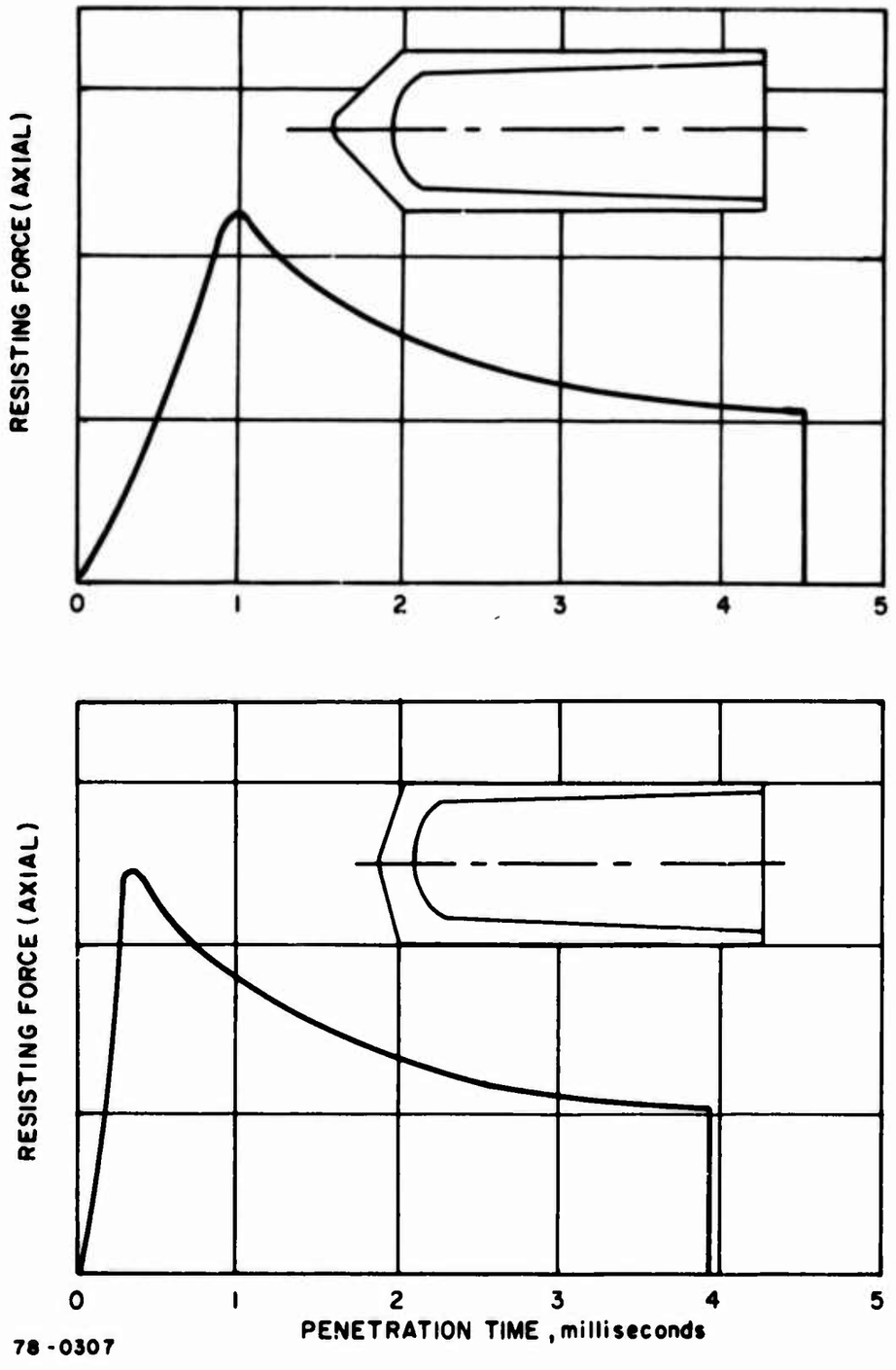

Figure 2 Predicted Typical Axial Forcing Functions for Penetrating Projectiles

finite element approach using the 1384 computer program. The formulation of the analytical model is shown in Figure 3. Typical results for a particular solution are shown in Figures 4 and 5 which compare the classical and the finite element approach for the free-free bar impacted at one end. For this case the striking mass is assumed rigid. The free-free rod has been simulated by 60 masses connected in series by springs. The rigid mass strikes the end of the rod at 71.5 in/sec. The impact ends when the initial compression wave reflects off the far end of the rod and returns to the struck end as a tension wave. From theory (Reference 7) the velocity (v) of the rigid mass after impact is

$$v = v_o\, e^{-2\alpha} = 71.5\; e^{-0.333} = 51.3 \text{ in/sec}$$

where v_o = striking velocity, and α is the reciprocal of the rigid body mass per unit area of the rod cross section (1/6 for this sample). Figure 4 shows the velocity history of the rigid mass using the finite element approach, indicating good agreement with theory. Again, from theory, the stress (δ) at the struck end of the bar just prior to impact determination is

$$\delta = E\epsilon = E\,(v_o/c)\; e^{-ct\,\alpha/L} = 728 \text{ psi (compression)}$$

where

ϵ = strain

E = modulus of elasticity

c = velocity of wave propagation

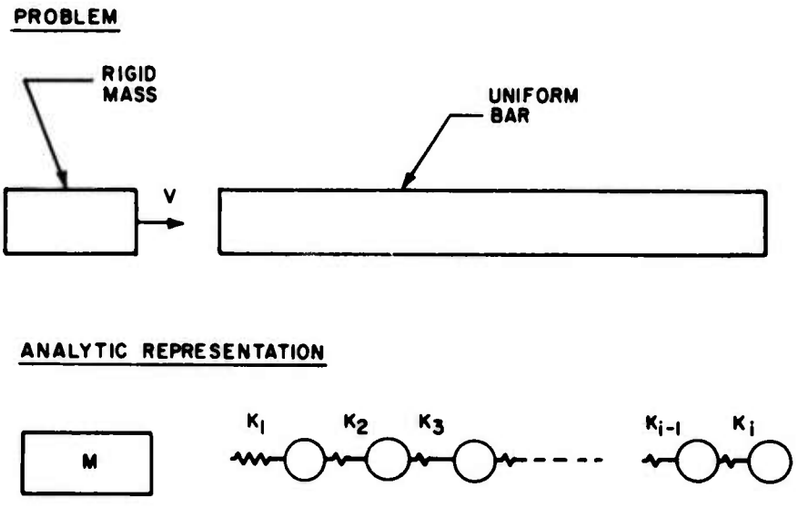

Figure 3 One-Dimensional Representation of Longitudinal Impact Problem

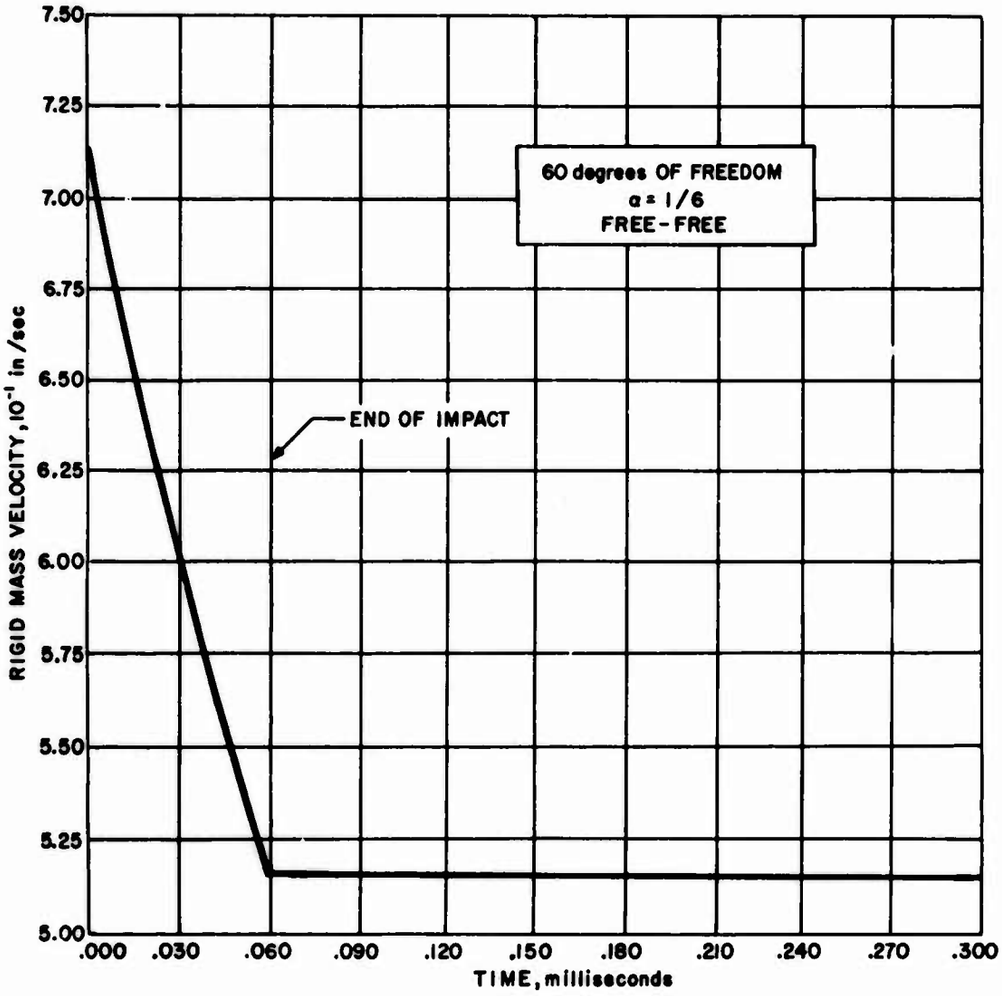

Figure 4 Velocity History of Rigid Mass

t = time

L = length of rod

The finite element solution for this stress is approximately 715 psi, as shown in Figure 5. Just after impact, the theoretical stress at this point is

$$\delta = E\left(\frac{-2v_o}{c}\right) e^{-\alpha} \sinh \alpha = -430 \text{ psi (tension)}$$

Figure 5 indicates a value of about 400 psi tension from the finite element solution.

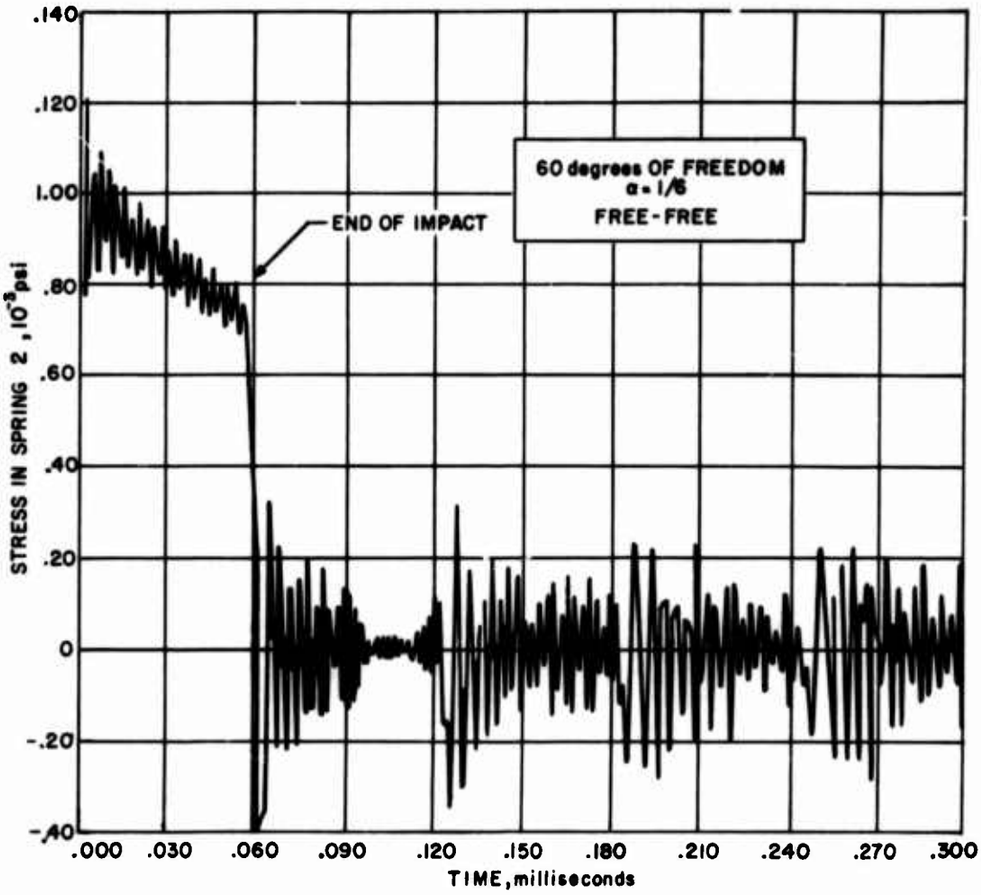

Figure 5 Stress History in Spring 2

Similar stress results are obtained throughout the length of the bar and show that the finite element approach does give very good agreement with theory.

It must be pointed out that although the solution includes both radial and longitudinal deformations, it accounts only for longitudinal stress waves in the system. The less important radial and flexural wave motions are ignored.

The output of the structural response computer programs presents the time histories of displacements and stress resultants. To assess the effects of the filler on the structure, the total loading condition must be examined. The total stress condition at a given location is composed of both axial and hoop (tangential) stresses. A commonly used criterion for determining when a material yields is the von Mises yield function. This is stated as

$$J^2 = S_1^2 + S_2^2 + S_3^2 - (S_1 S_2 + S_1 S_3 + S_2 S_3) \qquad (2)$$

where

J^2 = von Mises yield function

S_1 = axial stress

S_2 = hoop stress

S_3 = radial stress

Here, tensile stresses are positive, and compressive stresses are negative. Yielding occurs when J exceeds the static yield strength (S_0) of the material.

In the present situation the radial stresses may be neglected. They are negligible when comparing with the axial and hoop stresses. The yield function then reduces to

$$J^2 = S_1^2 + S_2^2 - (S_1 S_2)$$

The axial stress (S_1) and the hoop stress (S_2) both have two components: that caused by the axial load in the shell wall, which is (in the steady state case) the inertial load caused by the shell deceleration under an axial load; and that caused by the radial pressure exerted by the filler material, again (in the steady state case) an inertial load caused by deceleration of the filler material under an axial load.

The components of the stresses are defined as

S_{1a} = axial stress due to axial load in shell

S_{1r} = axial stress due to radial pressure caused by filler

S_{2a} = hoop stress due to axial load in shell

S_{2r} = hoop stress due to radial pressure caused by filler

The final form for the yield function is

$$J^2 = (S_{1a} + S_{1r})^2 + (S_{2a} + S_{2r})^2 - [(S_{1a} + S_{1r})(S_{2a} + S_{2r})]$$

Because the analysis is linearly elastic, the stresses due to the axial and the radial loads may be added directly (taking the signs of the stresses into account). Thus each component may be examined independently and then combined to form the total stress picture. By computing the stresses due to each loading separately, the individual effects of the axial load and the radial pressure (which is a function of the filler material properties) may be examined.

SECTION IV

RESULTS OF ANALYSES

A. MODEL AND FORCING FUNCTION FORMULATION

Using the method outlined in Section III, two separate bomb designs have been analyzed. One is a cylinder of uniform thickness and the other has a linearly varying thickness which is representative of typical penetrating bomb designs, where the shell wall is thicker at the front (impact) end. These two models are similar to the BLU-31B design. Each model is analyzed for a step axial load and a traveling radial pressure. Total stresses are a superposition of the stresses for each of these two loading conditions.

The two shells considered are shown in Figure 6. The shells are 60-inches long and 11.25 inches in diameter. The constant thickness case is 0.803-inch-thick, which is an average BLU-31B dimension. In the tapered case, the front end is 1.25-inch-thick, tapering linearly down to 0.50-inch-thick at the rear end.

The analytic finite element model to represent the cylindrical shells is shown in Figure 7. This model is used for both cases. It consists of 23 nodal circles spaced 3 inches apart except at the ends where the spacing is less to more accurately describe response at the shell boundaries. Each node has axial, radial, and rotational degrees of freedom. The first and last nodes are restrained from radial and rotational motion to simulate end cap effects. No restraints are imposed in the axial direction. As such, the model is free-free axially to represent the condition of a bomb traveling through the air.

With this analytic model defined, Avco Computer Program 2222 was utilized to obtain the mass and stiffness matrices required for the structural response programs. Coupling of the u, ω, and β coordinates is present in both of these matrices. For example, in the stiffness (K) matrix, motion of the u coordinate at nodal circle 12 induces u, ω, and β motion at nodal circles 11, 12, and 13. This type of coupling is present to some extent in the mass matrix as well. The size of the M and K matrices are 65 x 65.

Using these data, the 1384 structural response code was used. The first part of the program, 1384A, computes the natural frequencies and mode shapes of the system. Table I lists the first 12 natural frequencies of the system. Figure 8 shows the relative displacements of the u and ω coordinates for the first 12 modes, using the shell with uniform thickness. These indicate the relative magnitude of displacement in each mode (at each frequency) and indicates which motion predominates in a given mode (at a given frequency).

The first (lowest) frequency corresponds to the fundamental axial mode. In fact, the first modes are predominantly axial, with little radial or rotational motion. The first appreciable radial motion is found in the third mode, at 4635 cycles per second, and the radial motion predominates starting with the sixth mode. From here on, the modes are closely bunched over a narrow frequency range. The tapered cylinder frequencies are very close to those of the uniform cylinder and are just slightly higher in all instances. The lowest axial and radial mode frequencies should appear in the response analyses.

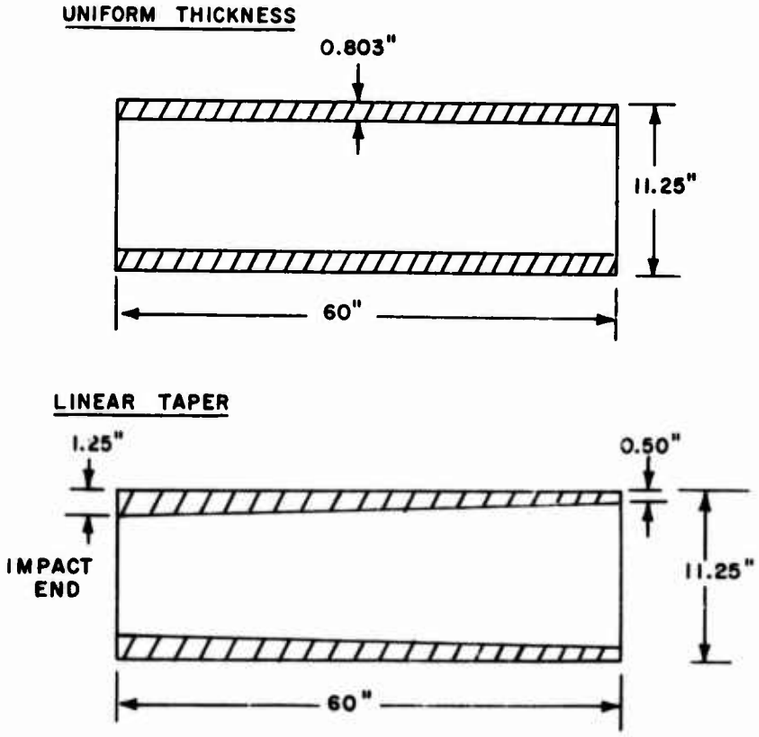

Figure 6 Shell Geometries

The forcing function inputs are computed on the basis of the Poncelet form for the resisting force during impact of a projectile with a concrete target. Using Equation (2) of Section III, the peak force is found, assuming an impact velocity of 1000 ft/sec, to be 5.74×10^6 pounds. This assumes

η = 25,000 psi

ρ = 0.225×10^{-3} lb sec^2/in^4 (150 lb/ft^3)

C_d = 2.0 (blunt-ended projectile)

A = 100 in^2

The weight of the projectile is approximately 702 pounds, composed of both the steel shell and the filler. This uses an average filler density of 0.062 lb/in^3. Under these conditions, the deceleration level is 8180 g's, and is held constant at that value. The forcing function values used for the step axial stress in the shell and the traveling radial pressure wave due to the filler are based on this 8180 g's deceleration value.

NODE	x, INCHES	SHELL THICKNESS, IN. UNIFORM CYL.	SHELL THICKNESS, IN. TAPERED CYL.
1	0	0.803	1.250
2	1		1.2375
3	3		1.2125
4	6		1.175
5	9		1.1375
6	12		1.10
7	15		1.0625
8	18		1.025
9	21		0.9875
10	24		0.95
11	27		0.9125
12	30		0.875
13	33		0.8375
14	36		0.80
15	39		0.7625
16	42		0.725
17	45		0.6875
18	48		0.65
19	51		0.6125
20	54		0.575
21	57		0.5375
22	59		0.5125
23	60		0.500

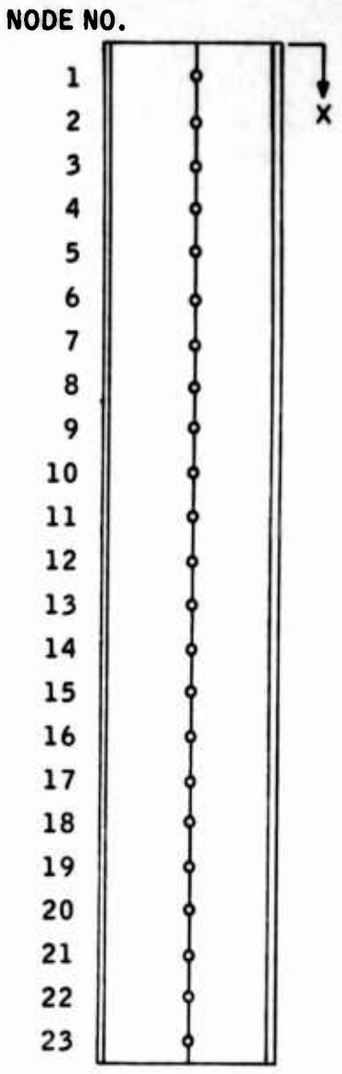

Figure 7 Finite Element Model -- Both Shell Geometries

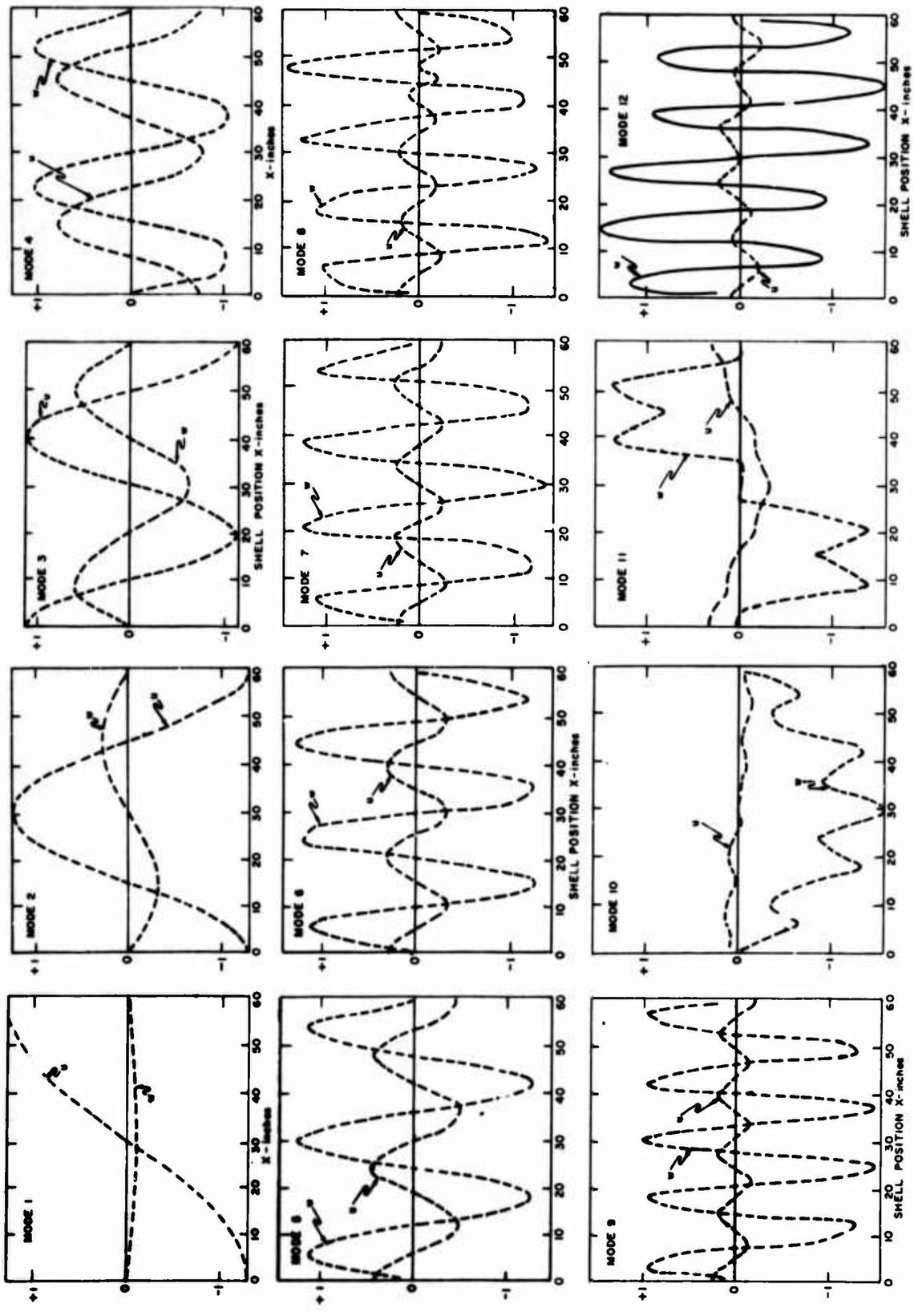

Figure 8 Modal Displacements, Uniform Cylinder

TABLE I. TWELVE LOWEST NATURAL FREQUENCIES OF THE SHELLS

Mode No.	Frequency (CPS) Uniform Cyl	Tapered Cyl	Predominant Motion
1	1626	1701	u
2	3216	3294	u
3	4635	4727	u, w
4	5491	5589	u, w
5	5790	5892	u, w
6	5922	6028	w
7	6021	6131	w
8	6125	6241	w
9	6248	6370	w
10	6272	6382	w
11	6360	6470	w
12	6409	6548	w

The resisting force acts on both the steel shell and the filler material. With a shell weight of 465 pounds, the axial force felt by the shell is 3.8×10^6 pounds. This value, based on the ratio of shell weight to total projectile weight, is used for the axial loading condition in the shell.

The corresponding stress acting in the filler is computed by assuming that the front face of the filler material experiences the same particle initial velocity as the shell. This is determined from the general relation

$$\delta = \rho C V \tag{3}$$

where

δ = stress magnitude

ρ = material density

C = speed of sound in the material = $\left(\frac{B}{\rho}\right)^{1/2}$

B = bulk modulus or modulus of elasticity of the material

V = particle velocity

Knowing the axial step stress imposed upon the shell, Equation (3) is used to compute the initial particle velocity in the shell at the impact end. The filler material is then assumed to have this same initial particle velocity at time zero when impact starts. This fixes the stress level, using Equation (3), which acts at the end of the filler and travels down the length of the shell. The axial pressure acting in the filler exerts a radial pressure of equal magnitude along the shell-filler interface. The rear surface of the filler (at the aft end of the shell) is considered to be a free surface, so the axial pressure wave reflects forward as a tensile wave which cancels out the compressive stresses already in the filler. Actually, the degree of fixity at the rear end bears close scrutiny. If the base plate (end cap) is firmly in contact with the filler material, the compressive wave traveling in the filler would meet the base plate and reflect forward as a compressive wave. In addition to this, the base plate is oscillating itself because the axial stress wave moving down the shell wall would have reflected off the base plate and induced motion in it. Since the compressive wave travels faster through the steel than through the filler, this motion would have already begun by the time the filler compressive wave reached the end. This complicated interaction between the base plate, the shell, and the filler was ignored in the present study. A more detailed explanation of this is presented in Section V.

It is known that a substantial amount of damping does exist in these filler materials. Due to a lack of information on quantitative damping properties of filler materials, a value of 5 percent structural damping was assumed in the formulation of the radial pressure wave front magnitudes.

The first longitudinal natural frequency of the filler material is 500 cycles per second (its period is twice the length of the cylinder divided by the sound speed in the filler). The wave front magnitude (P) was assumed to have the value

$$P = P_o e^{-\gamma \omega t}$$

where

P_o = filler compressive pressure at time of impact

γ = 0.05, corresponding to 5 percent damping

ω = first longitudinal frequency in radians per second

t = time after impact, seconds

As a result of the damping, the wave front pressure (P) continually decays according to the above relation. It is felt that this 5 percent value is probably low (conservative) but is at least indicative of actual filler behavior. For the steel shell casing, 1 percent modal damping was used. The effects of damping are seen in the response plots.

The filler material used for th basic response analyses reported in the next section has a density of 0.062 lb/in^3 and a speed of sound of 60,000 in/sec. This corresponds to a typical Comp B filler with between 1 and 2 percent wax.

B. RESULTS - UNIFORM THICKNESS CYLINDER

The 1384B transient structural response program was utilized to obtain time histories of displacements and stresses for the cylinder of uniform thickness subjected to axial and radial loads. The important results of interest are the axial and hoop stresses acting in the shell.

The 1384 program plots desired results in addition to the regular printout. Values plotted are stress resultants with units of pounds per inch. The actual stresses are obtained by dividing the stress resultants by the shell thickness. The analytic solutions have been carried out for 4 milliseconds. Since the steel has a sound speed close to 200,000 in/sec, a shock wave will travel the length of the 60-inch shell and back to the front almost seven times in this time period. The filler has a sound speed of 60,000 inches per second and will thus travel up and back two times. With 1 percent modal damping in the shell structure and 5 percent damping in the filler pressure wave, 4 milliseconds should suffice to determine peak stresses.

Results have been obtained along the entire length of the cylinder. Plotted output for the midpoint along the cylinder, 30 inches from both the front and rear ends, are presented in this report. They are typical and representative of the output for all points along the cylinder. Additionally, this location feels essentially the same peak stresses as points elsewhere in the cylinder.

Figures 9 and 10 present the axial stress resultants due to the axial load and the radial pressure, respectively. The peak axial stress resultant is a compressive 130,000 lb/in on the third round trip of the axial stress wave.

The axial step stress input at the impact end is 144,000 psi, which is a stress resultant of 116,000 lb/in. This is the peak magnitude which should be felt all along the length of the cylinder. The reason that the finite element solution gives a slightly different peak value is partly because not enough modes of the analytical system were considered. Theoretically, an infinite number of degrees of freedom are required to produce the square wave type of response which actually occurs for the axial load condition. A resemblance of this form (square wave) is evident in Figure 9. Another reason for the difference is that coupling due to radial motion causes some perturbations. This point is discussed further in Section V.

The frequency of the maximum compressive stresses is about 1600 cps, which matches the first natural frequency of the system as tabulated in Table I. Inspection of the axial stress resultants due to the radial pressure load, as plotted in Figure 10 reveals that the maximum value does not exceed a compressive value of -5200 lb/in. This is negligible compared to the 130,000 peak value reached due to the axial load. It is therefore logical to ignore this component of stress in making any generalization regarding the effects of the filler.

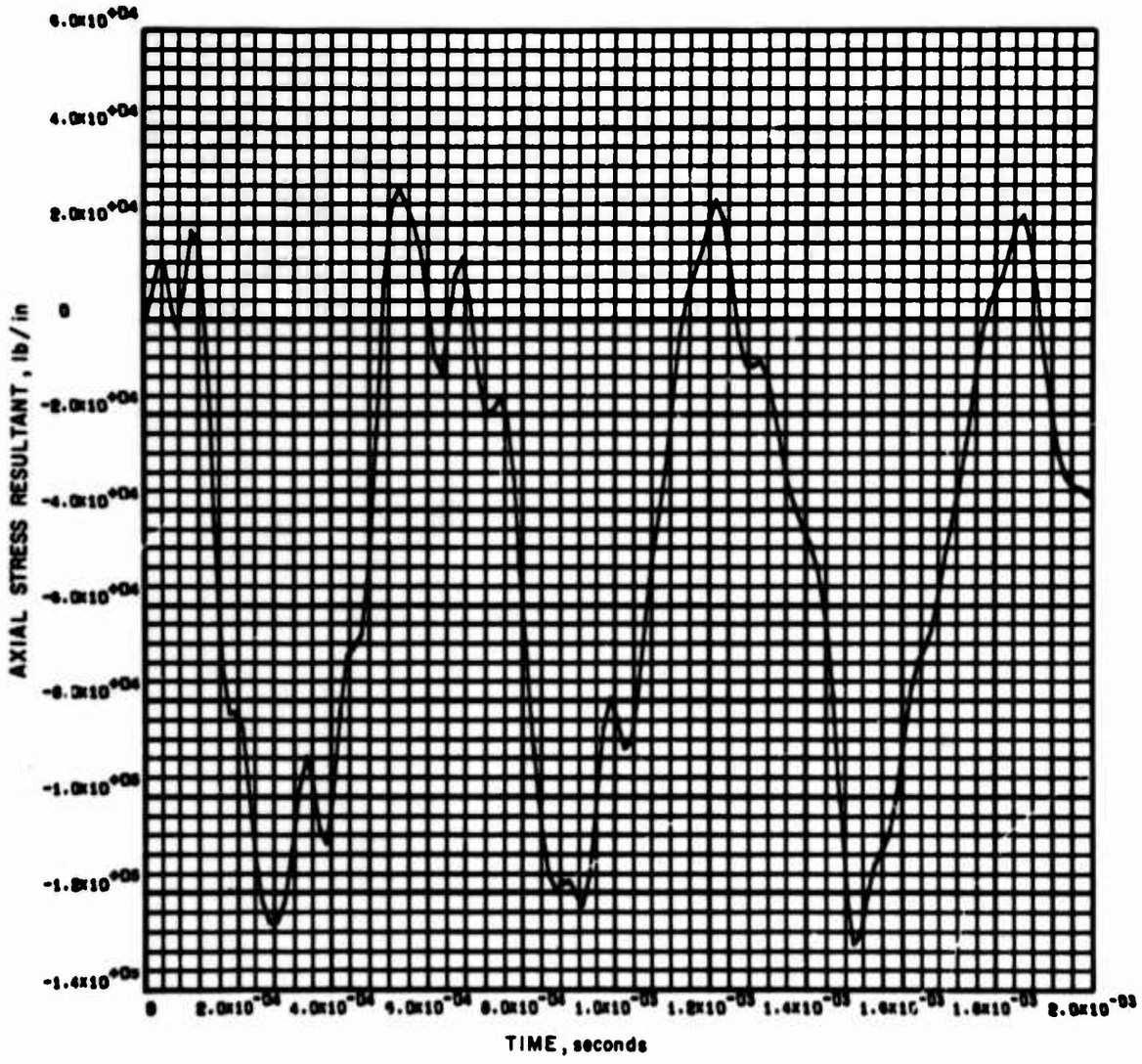

Figure 9 Axial Stress Resultant -- Axial Load -- Midpoint of Uniform Cylinder

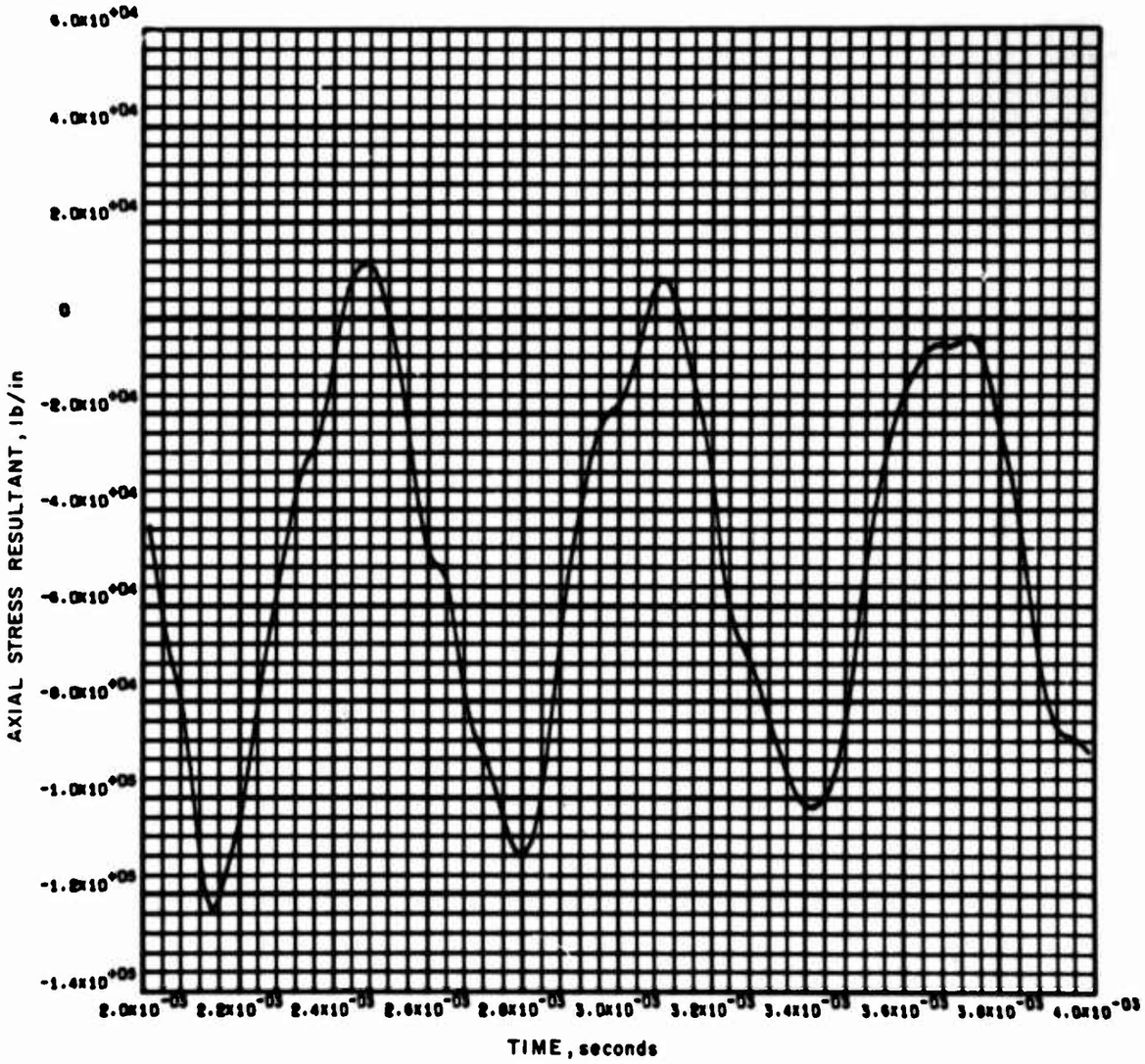

Figure 9 (Concl'd)

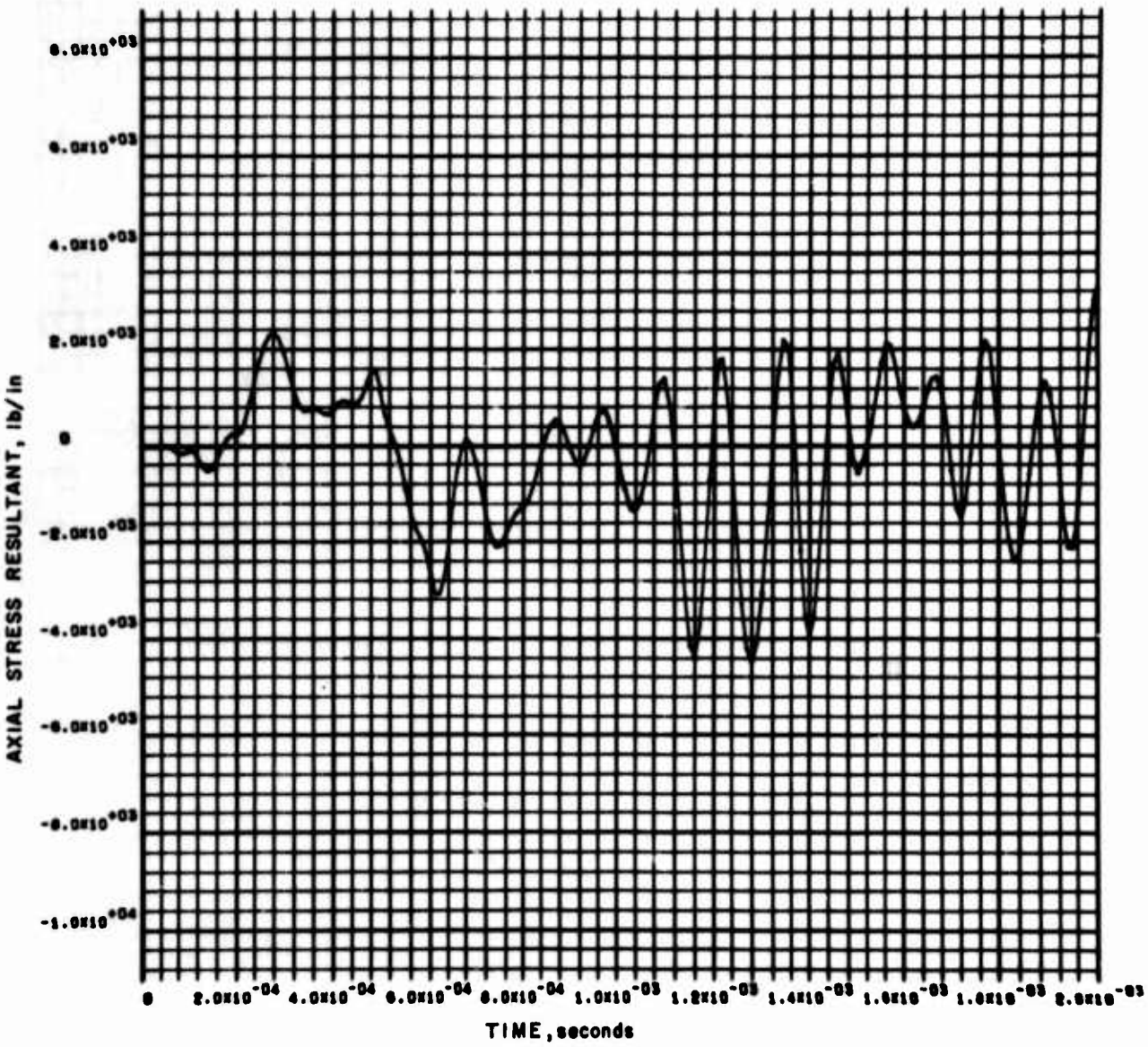

Figure 10 Axial Stress Resultant -- Radial Load -- Midpoint of Uniform Cylinder

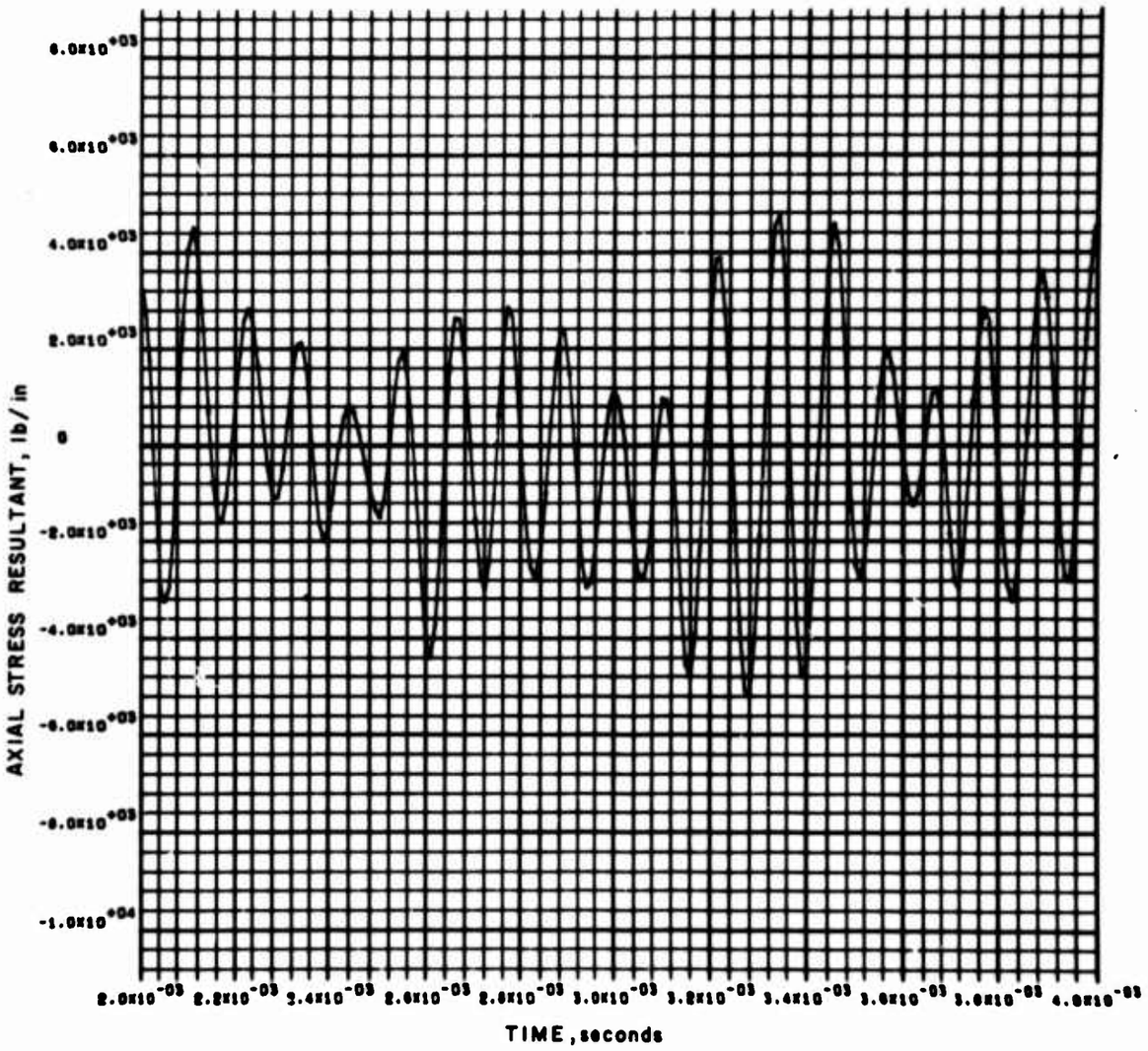

Figure 10 (Concl'd)

The hoop stress resultants are plotted in Figures 11 and 12 for the axial load and radial pressure conditions. The axial load induces a peak value of tension at 25000 lb/in and a peak compressive value of -12000 lb/in. The oscillations are damping out quite rapidly by 4 milliseconds after impact. Several frequencies occur in this plot, but oscillations appear to occur in the 6000 cps range.

The hoop stress resultant due to the radial pressure wave is shown in Figure 12. Two distinct peak tensile hoop stress resultants, at about 80,000 lb/in, occur when the traveling pressure wave passes the 30-inch location as it moves aft on the first and second trips. The presence of two or more close natural frequencies in the oscillatory response is seen from the "beating" phenomenon (where oscillations tend to be alternately reinforced and cancelled out). This is occurring in the region of 8000 cps. It is interesting to note that the oscillations are somewhat more severe during the second round trip of the radial pressure wave. This is because oscillations due to the first passage have not decayed appreciably (with 1 percent modal damping) by the time the second passage of the radial wave occurs.

An additional computer run was made to combine the two loading conditions into one solution. This in effect automatically combines the stresses into total axial and hoop stress resultants. These results for the axial and hoop stress resultants are presented in Figures 13 and 14, respectively. The peak axial stress resultant is unchanged from the axial load only case, at -130,000 lb/in. In fact, the entire plot is almost unchanged from that presented in Figure 9 for the axial load case. This shows the negligible effect of the radial pressure on the axial stress resultant.

The total hoop stress resultant plot of Figure 14 is similar to the radial pressure plot of Figure 12 with minor modifications. The initial peak value has dropped from 78,000 to 72,000 lb/in. The second maximum value has increased very slightly, from 82,000 to 84,000 lb/in.

The phasing of the various stress components is very important in determining peak stress values. Phasing of the responses means combining the stress values at a specific time. By doing this, the peak axial load value is not added to the peak radial pressure value unless they both occur at the same time. For this filler material used in the analysis, the total axial stress was unchanged when combining the two loading conditions, and the peak hoop stress resultant rose by only 2000 lb/in. If the peak hoop value due to the axial load was added directly to the peak value due to the radial load, the total hoop stress resultant would be 107,000 lb/in, an increase of 27 percent. These hoop values could become additive if the phasing of these stress responses had changed only slightly.

In other words, if the results in Figure 11, were shifted only 0.08 milliseconds to the left, the +16,200 axial load value shown at 0.66 milliseconds would add to the +78000 value shown in Figure 12 for the radial pressure loading condition. Such a possibility would occur if the sound wave speed in the filler were slightly faster than 60,000 in/sec, causing the shell response peaks to occur earlier than shown in the figures.

A summary of the peak stress resultants is given in Table II. Also given are the total stress resultants, combining the axial and the hoop stress components. By combining the peak axial load and the peak radial pressure, which ignores the

phasing of the responses, the total stress resultant is 211,000 lb/in. This is 12 percent higher than the total stress resultant obtained by the combined axial load and radial pressure run.

As shown in Table II, the effect of the filler is very significant. It induces essentially no axial stress into the system but creates a large hoop stress, peaking at a tensile 82,000 lb/in. This value may be ratioed directly with filler material properties. The input radial stress δ is expressed as

$$\delta = (B\rho)^{1/2} V$$

Here, B is the bulk modulus of the material, and ρ is the material density. For a given initial particle velocity V, the input stress varies as $(B\rho)^{1/2}$. Using the relationship, the peak hoop stress resultants due to the filler (via the radial pressure loading) may be found for any $(B\rho)^{1/2}$. Table III shows relative magnitudes for three possible Comp B explosive compositions. It is seen that the radial pressure for this explosive could vary from 76 to 113 percent of the value used in the detailed analyses. Hoop stress resultants would be adjusted accordingly to account for these changes. The axial stresses would remain unchanged as they are essentially unaffected by the radial pressure, for all practical purposes.

C. RESULTS - TAPERED THICKNESS CYLINDER

Results for the cylinder of tapered thickness are very similar to those of the uniform thickness cylinder. The only difference in the two cases is the tapered thickness, from 1.25 inch at the front (impact) end, to 0.50 inch at the rear end. Otherwise, geometry, material, and initial loading conditions were identical.

Again, typical results are presented at the midpoint of the cylinder, half-way from each end. The thickness here is 0.875 inch, as opposed to the 0.803-inch thickness in the uniform cylinder case. Figures 15 and 16 show the axial stress resultant responses for the axial force and radial pressure loading conditions. For the axial load, the peak axial stress value is a compressive -107,000 lb/in, occurring on the third round trip of the axial stress wave. The effects of damping are evident as time progresses. The corresponding axial stress resultant for the radial pressure wave has a maximum compressive value of -4500 lb/in, which is very small compared to the axial force counterpart. The radial oscillations are quite apparent, but the levels of its peak value are relatively low and may be neglected.

The hoop stress resultants for the axial and radial pressure loading conditions are given in Figures 17 and 18. As was true in the uniform cylinder analysis, the maximum tensile value of 20,000 lb/in for the axial load case occurs during the first transit of the wave. The oscillations are in the 5000 to 6000 cps region, which means that only minor shifts in the phasing of these responses could change stresses from compression to tension, thus altering total hoop stress magnitudes appreciably.

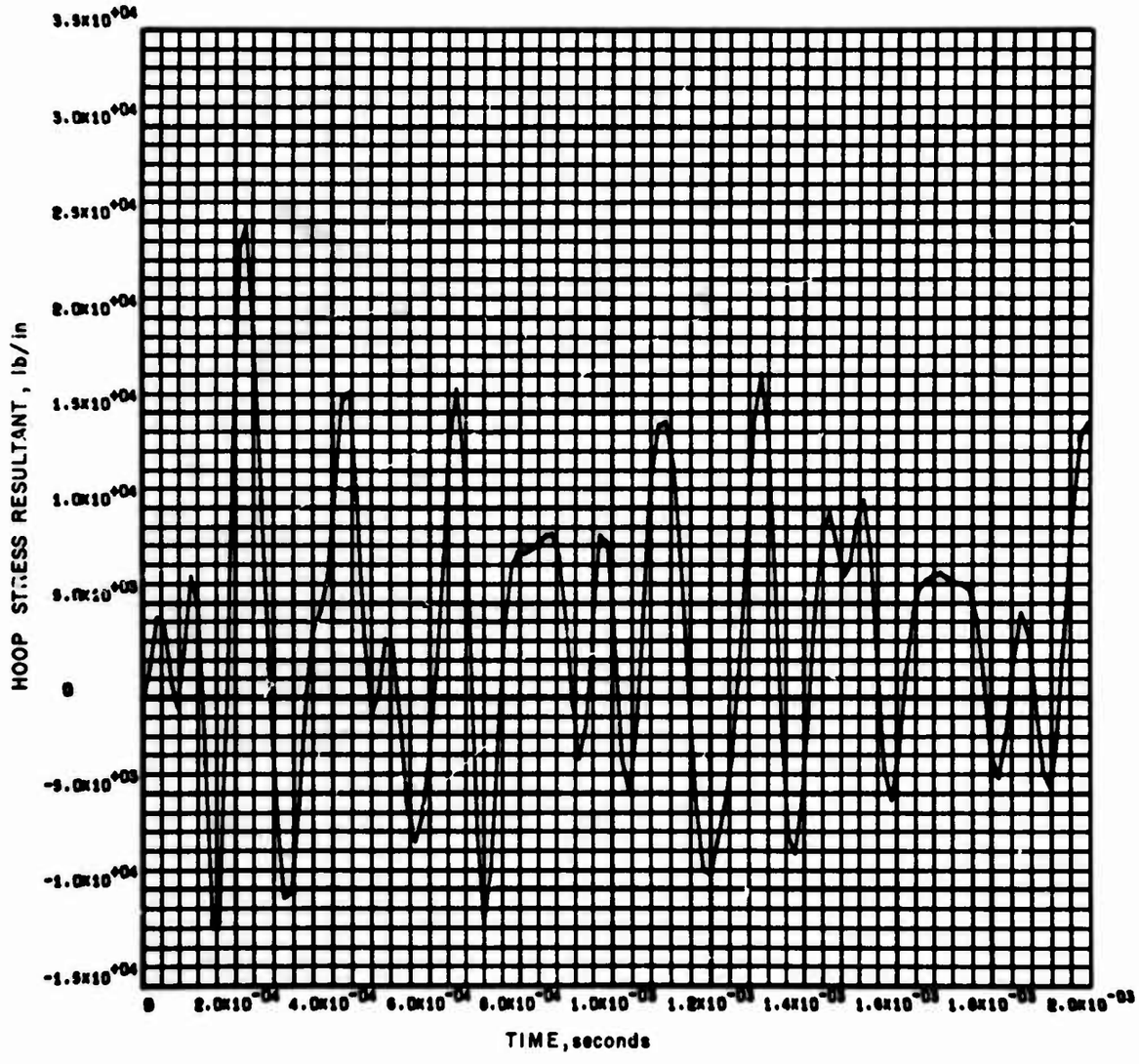

Figure 11 Hoop Stress Resultant -- Axial Load -- Midpoint of Uniform Cylinder

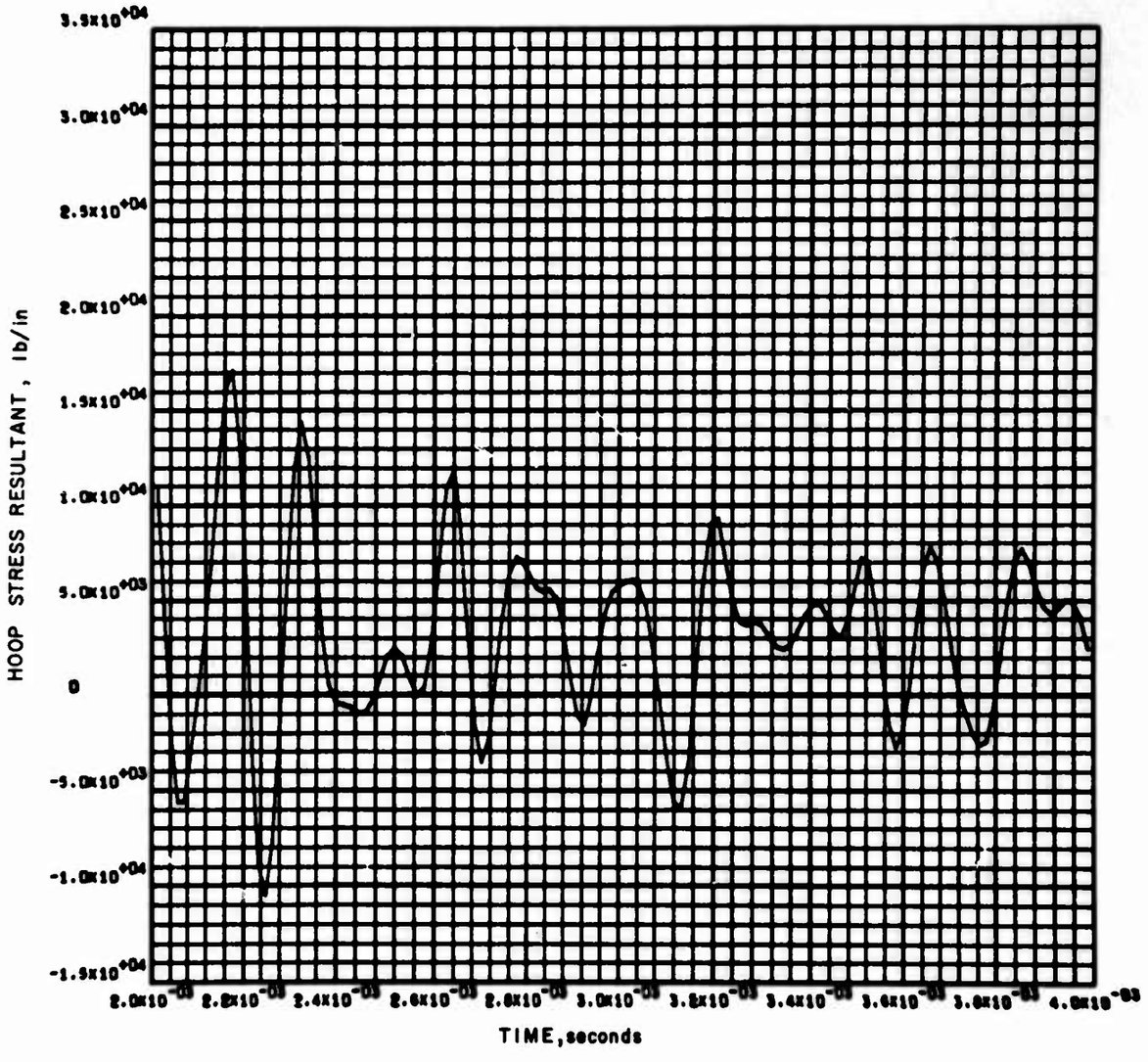

Figure 11 (Concl'd)

NOT REPRODUCIBLE

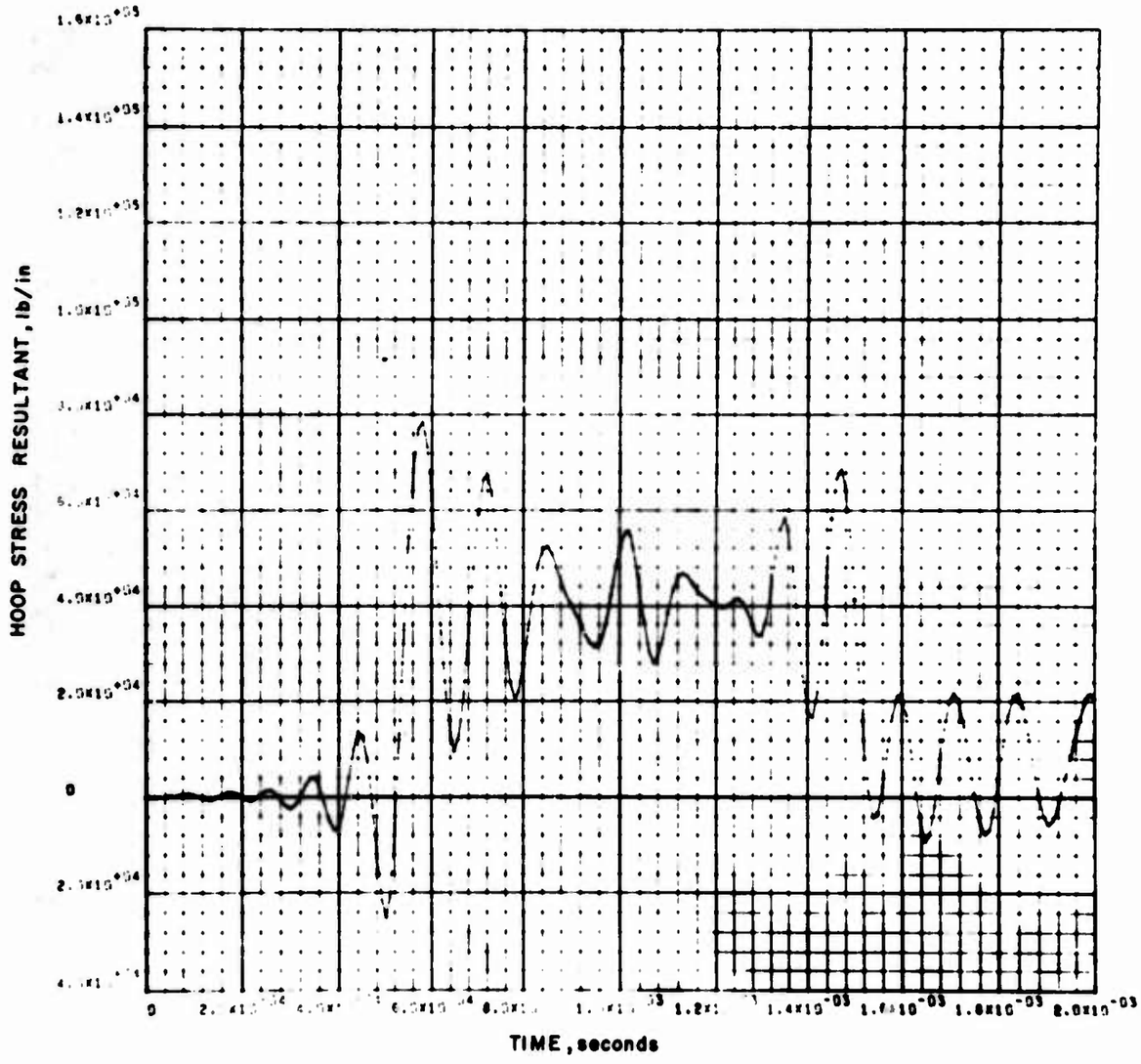

Figure 12 Hoop Stress Resultant -- Radial Load -- Midpoint of Uniform Cylinder

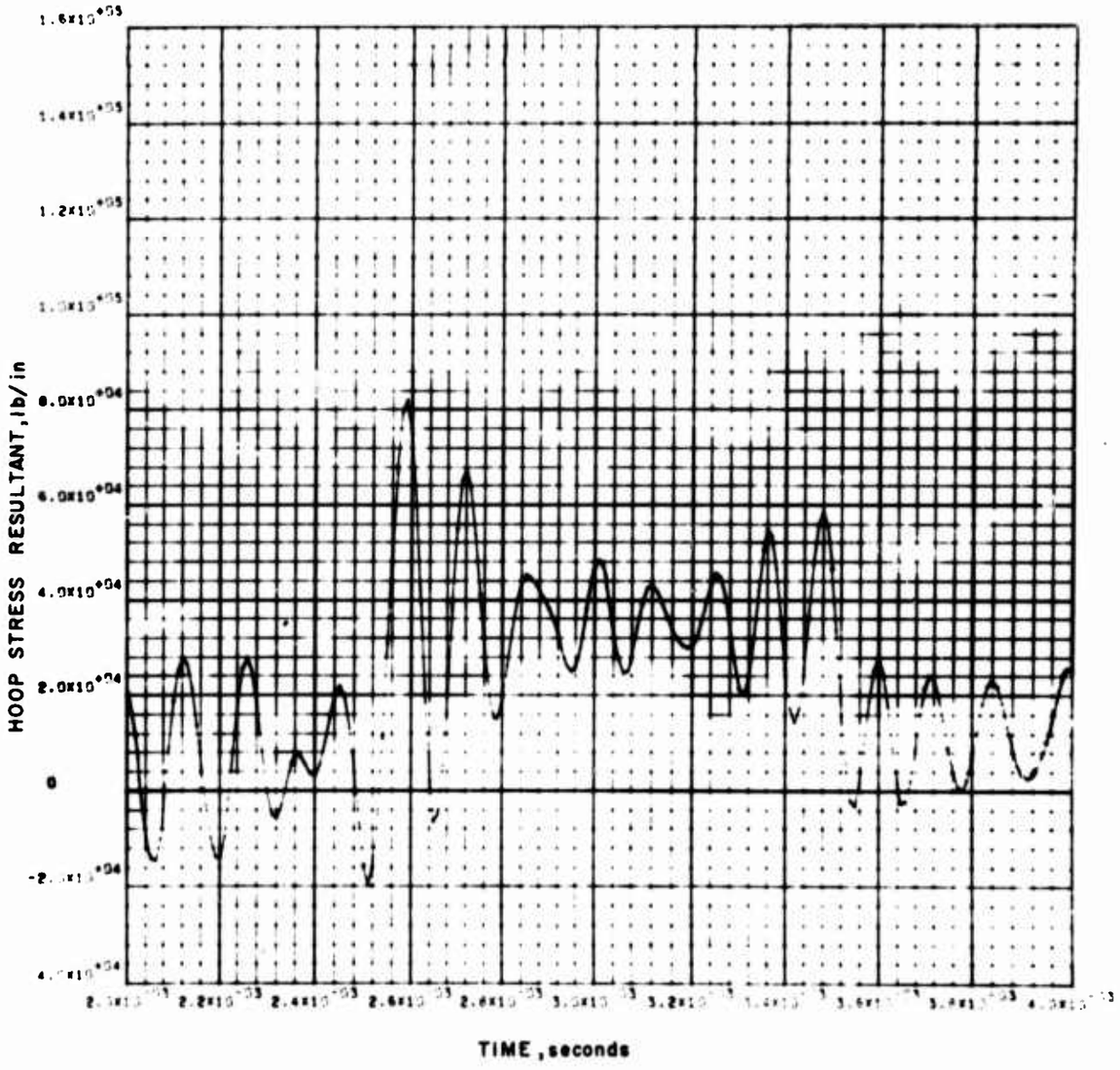

Figure 12 (Concl'd)

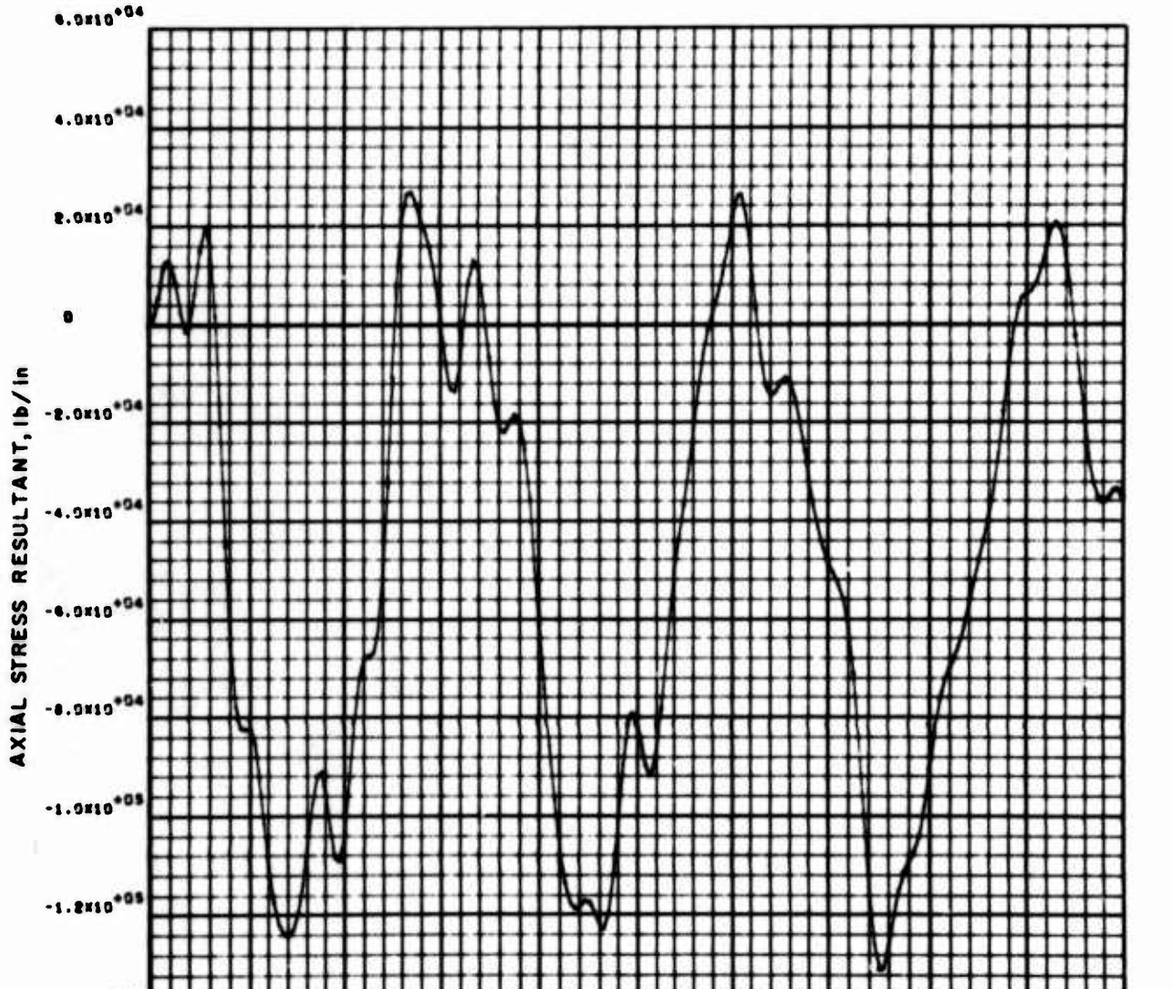

Figure 13 Axial Stress Resultant -- Axial and Radial Loads -- Midpoint of Uniform Cylinder

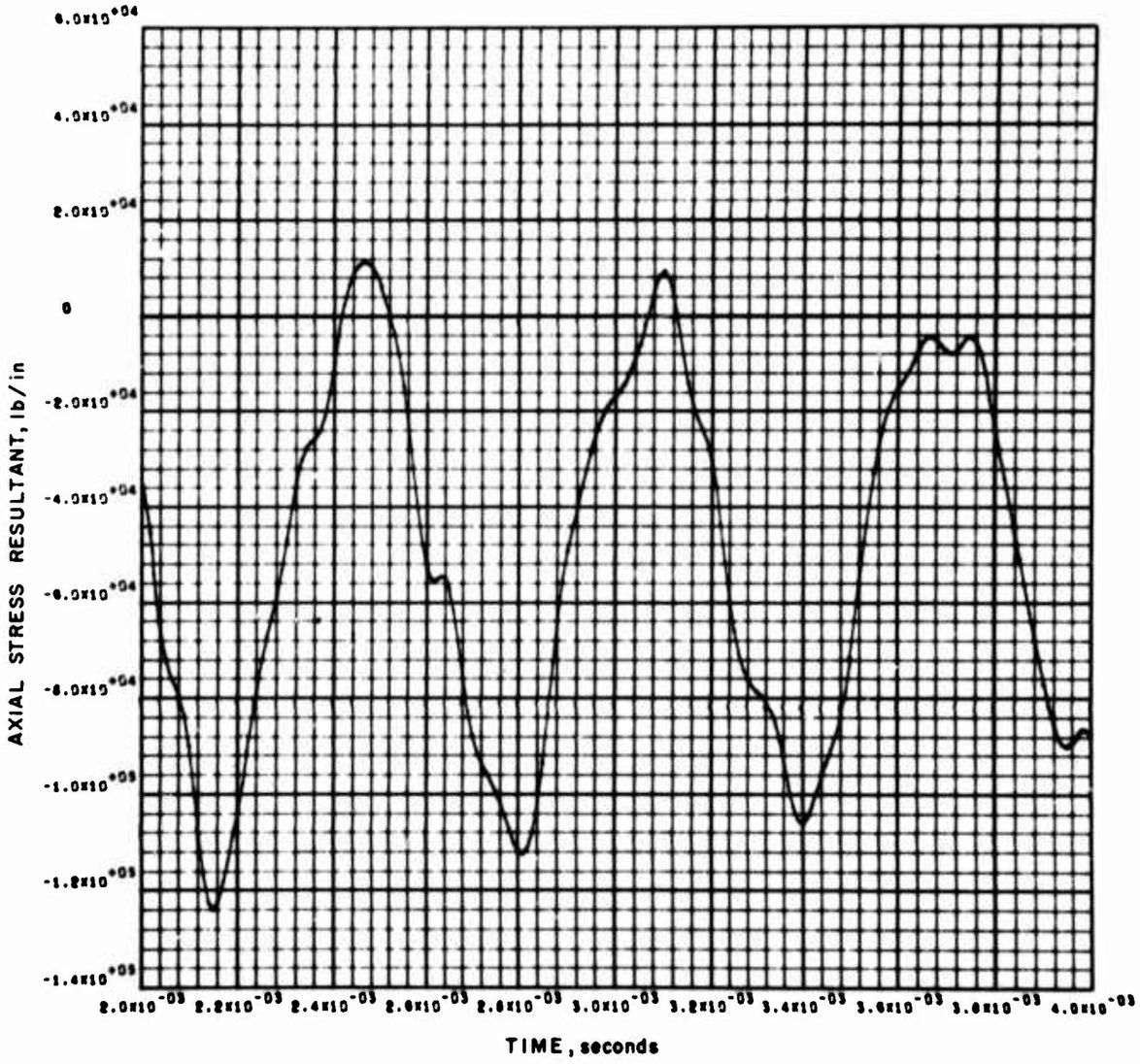

Figure 13 (Concl'd)

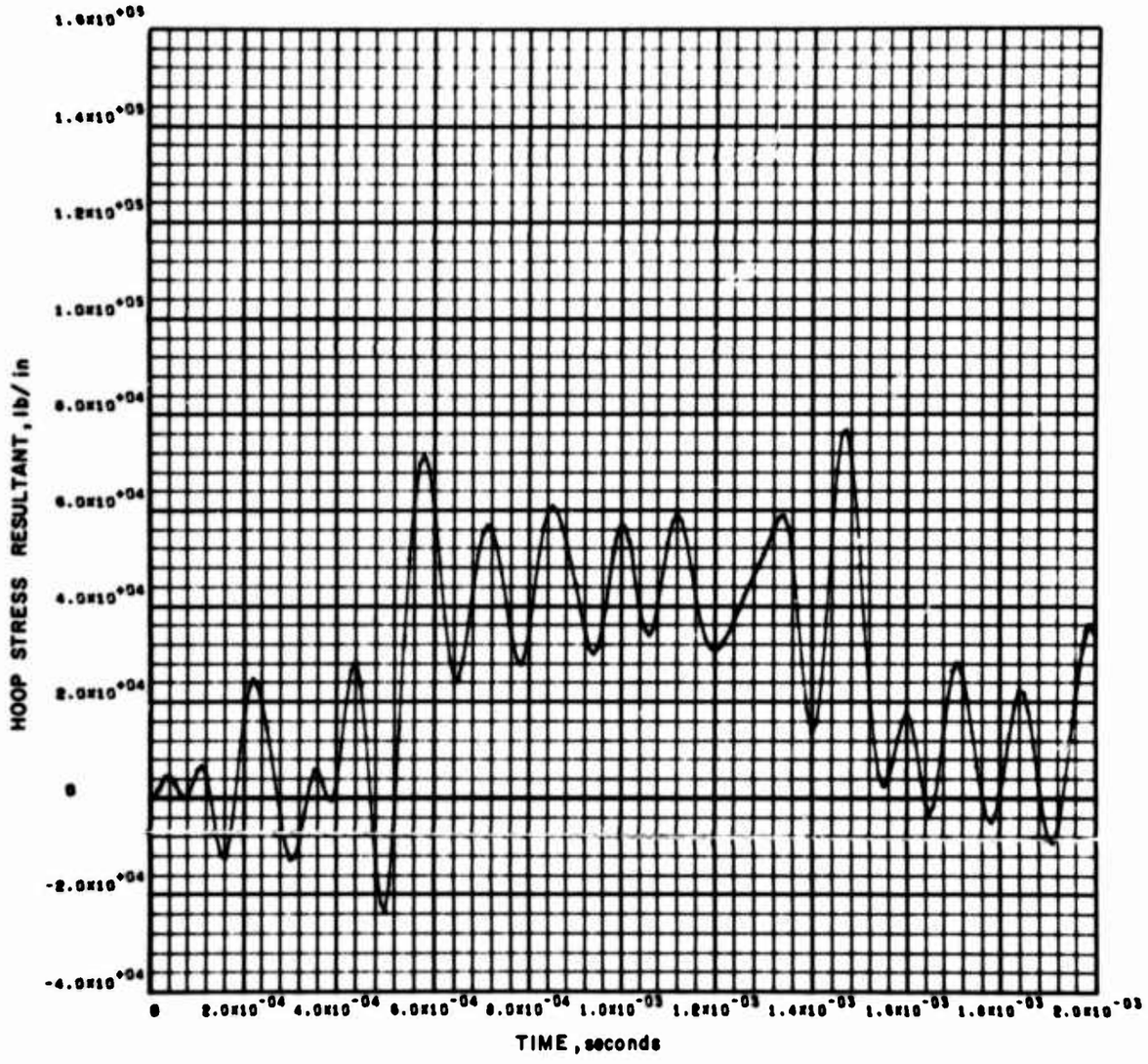

Figure 14 Hoop Stress Resultant -- Axial and Radial Loads -- Midpoint of Uniform Cylinder

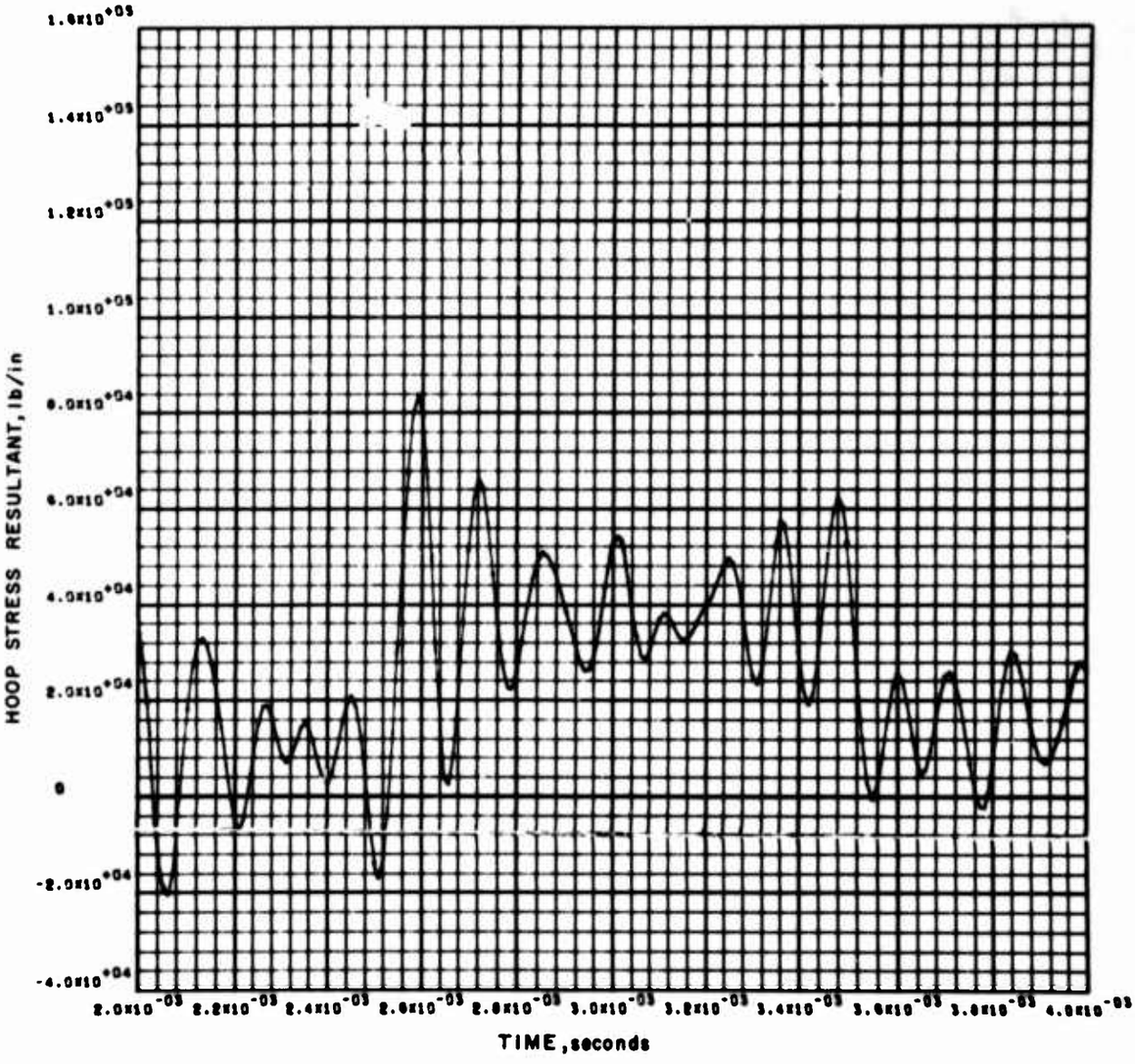

Figure 14 (Concl'd)

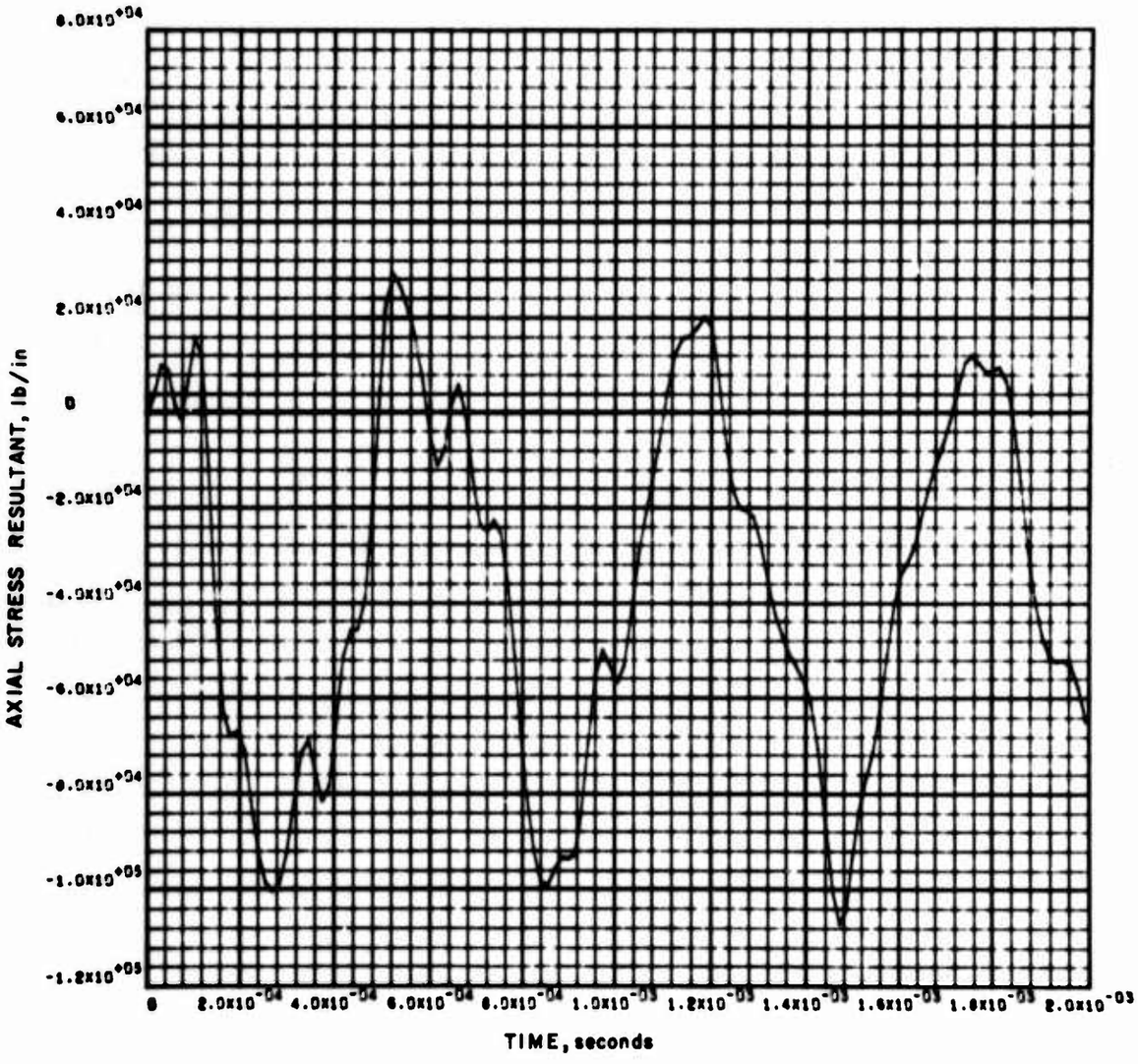

Figure 15 Axial Stress Resultant -- Axial Load -- Midpoint of Tapered Cylinder

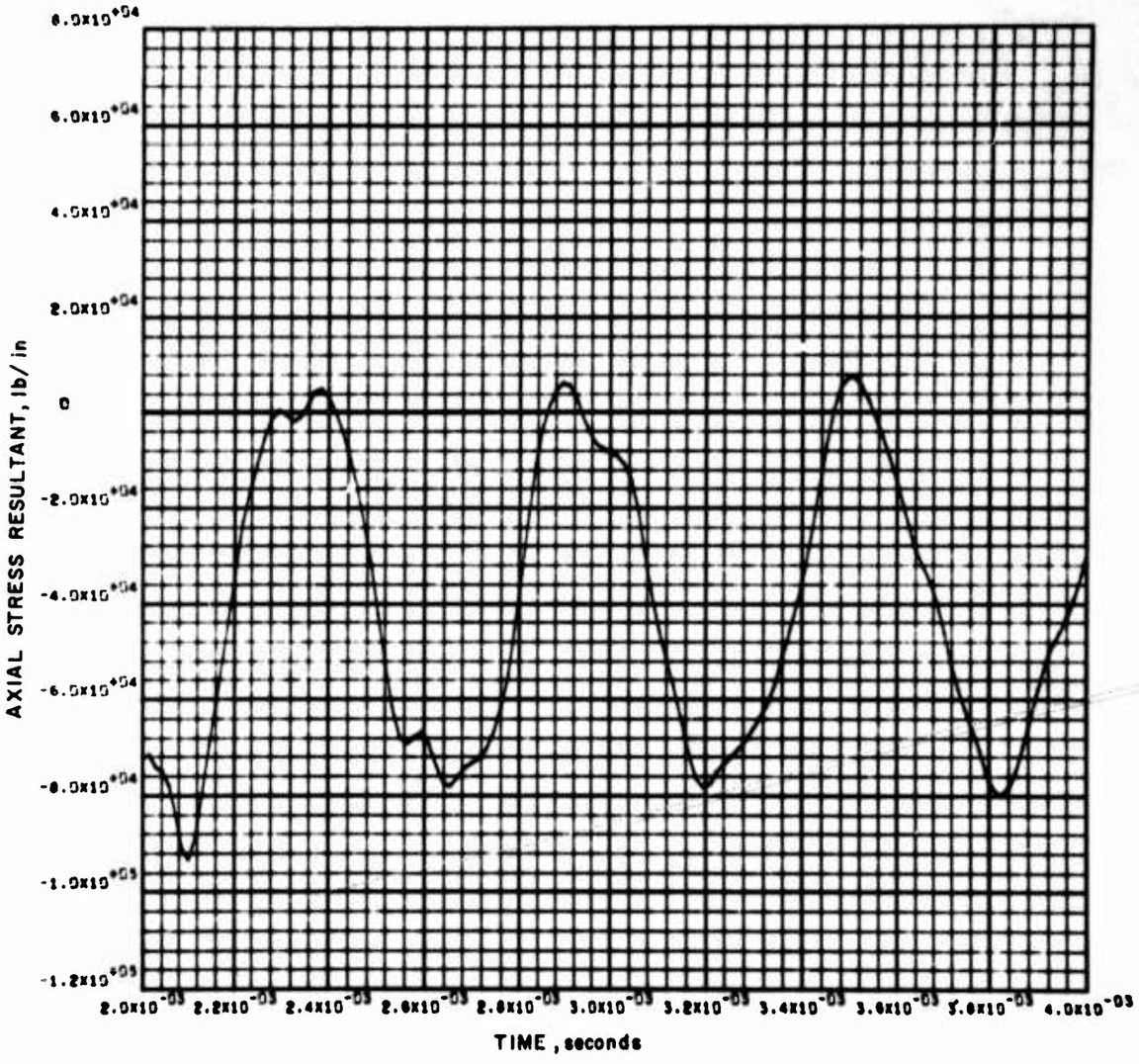

Figure 15 (Concl'd)

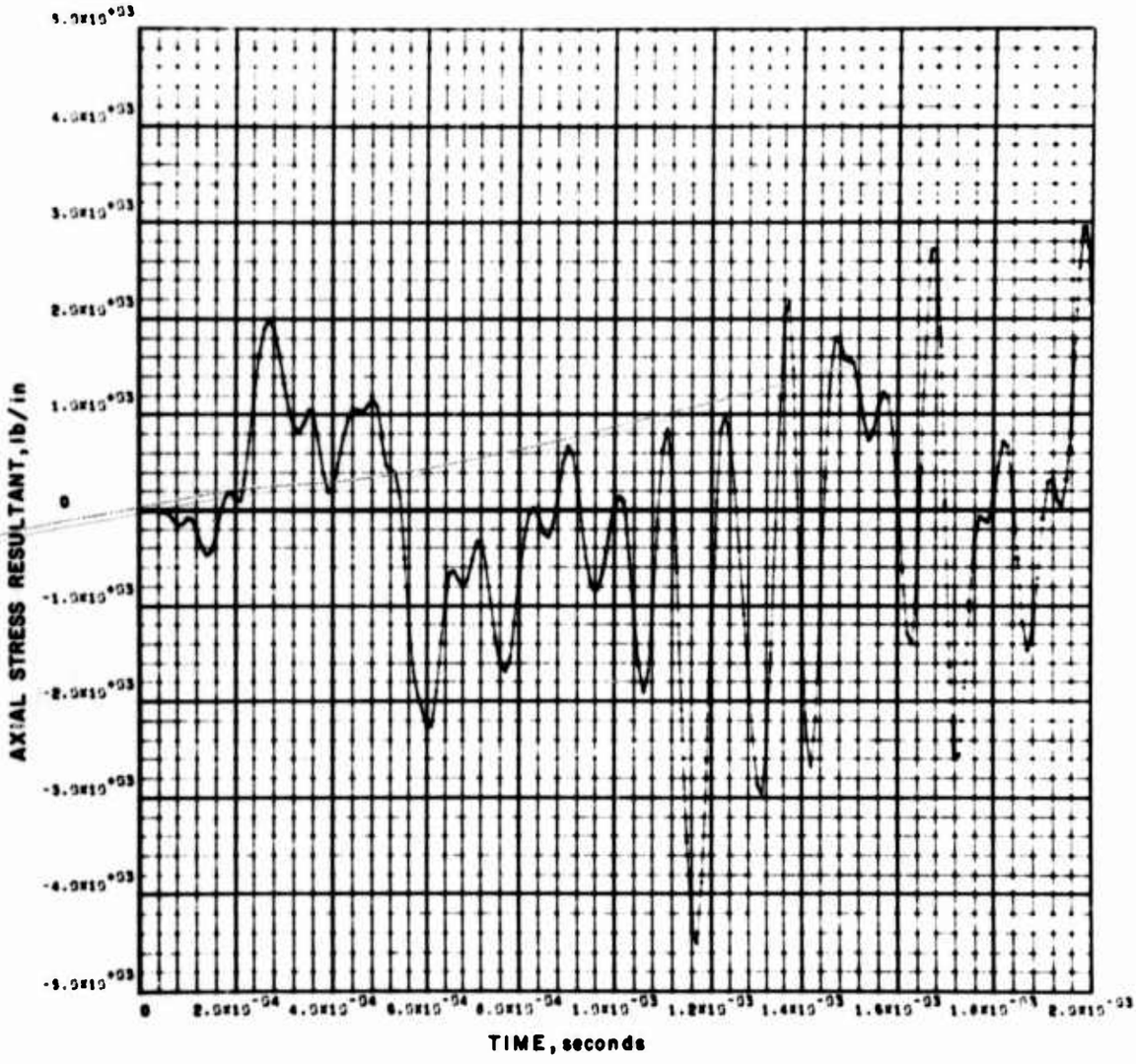

Figure 16 Axial Stress Resultant -- Radial Load -- Midpoint of Tapered Cylinder

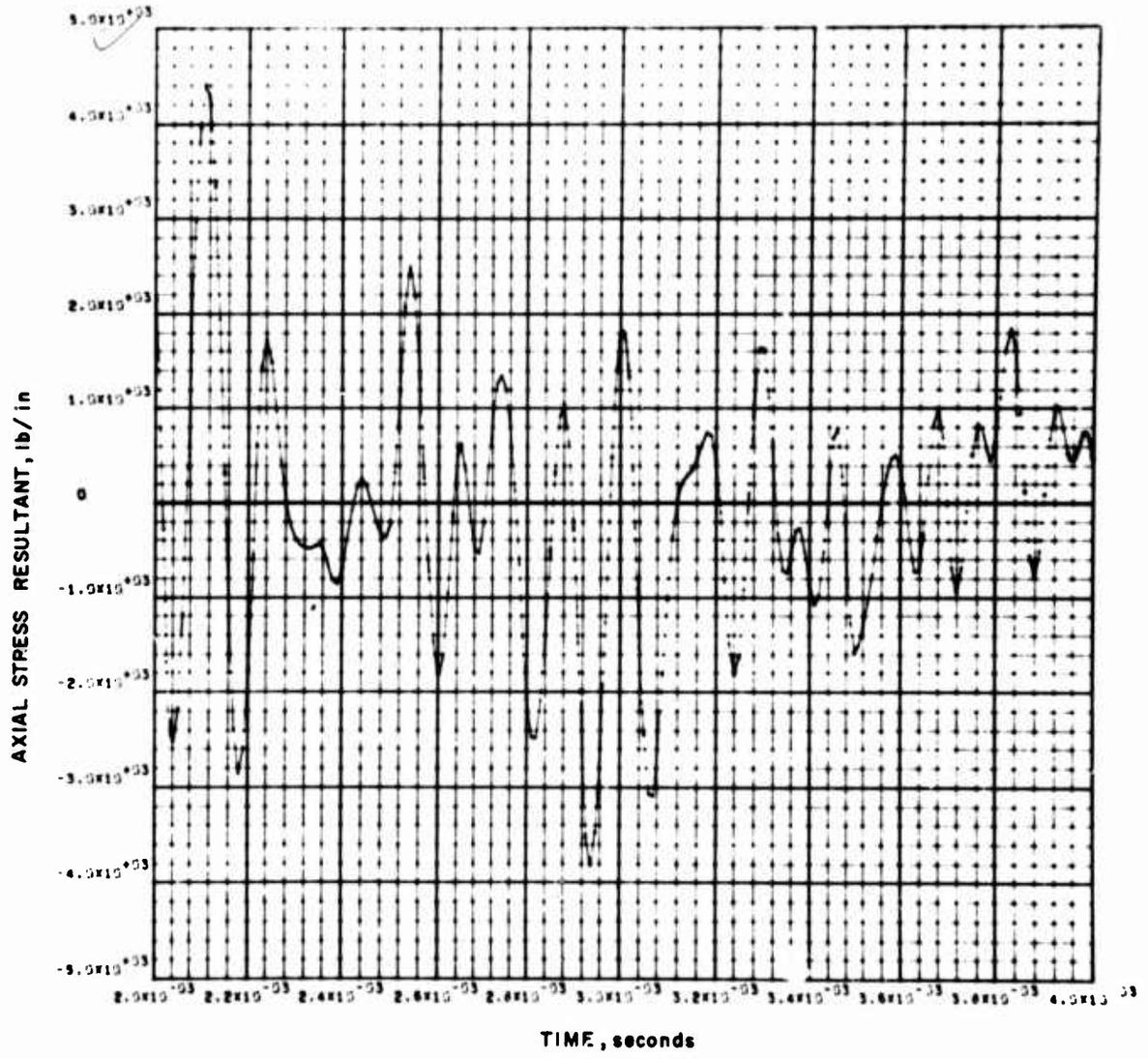

Figure 16 (Concl'd)

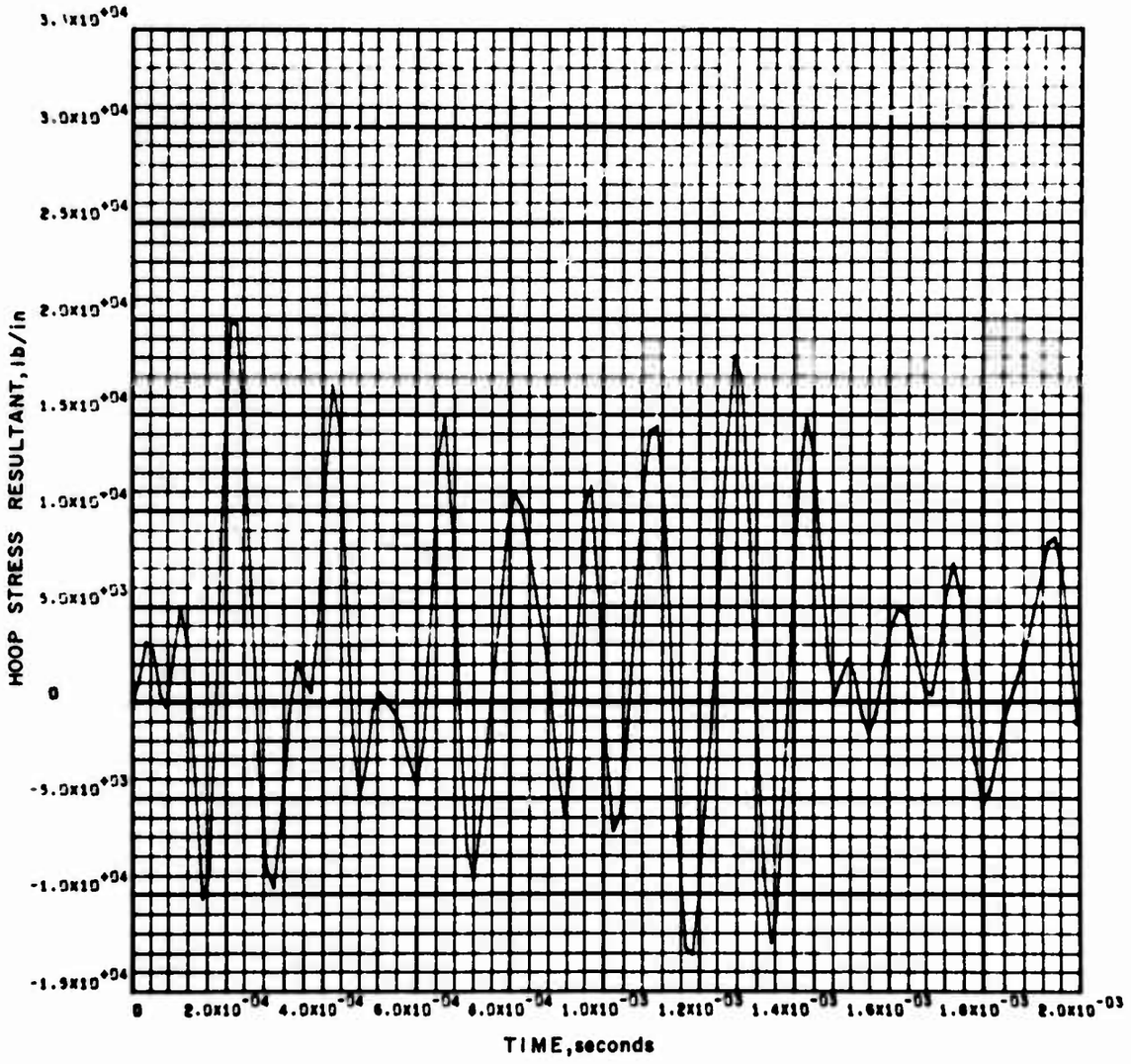

Figure 17 Hoop Stress Resultant -- Axial Load -- Midpoint of Tapered Cylinder

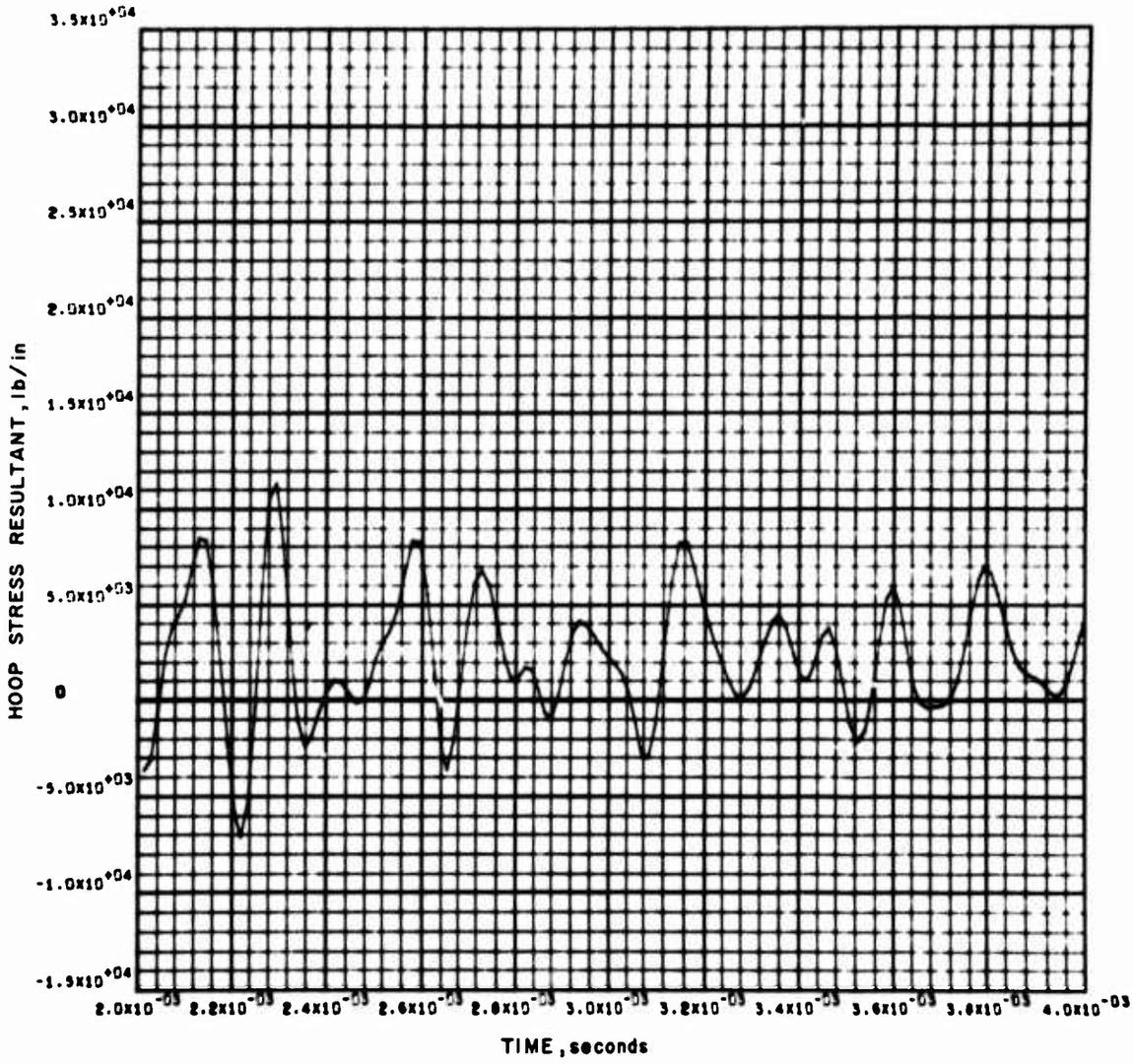

Figure 17 (Concl'd)

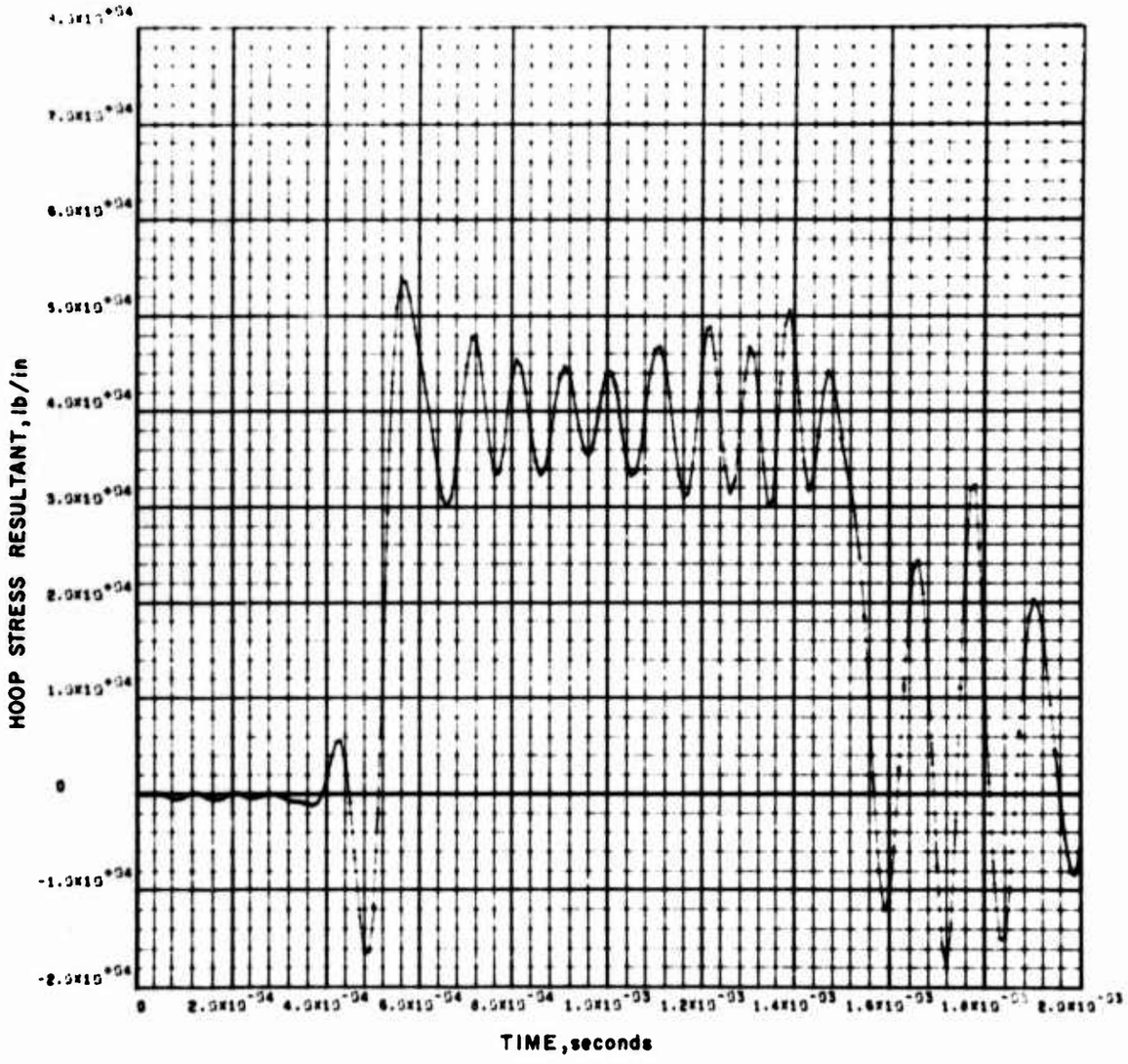

Figure 18 Hoop Stress Resultant -- Radial Load -- Midpoint of Tapered Cylinder

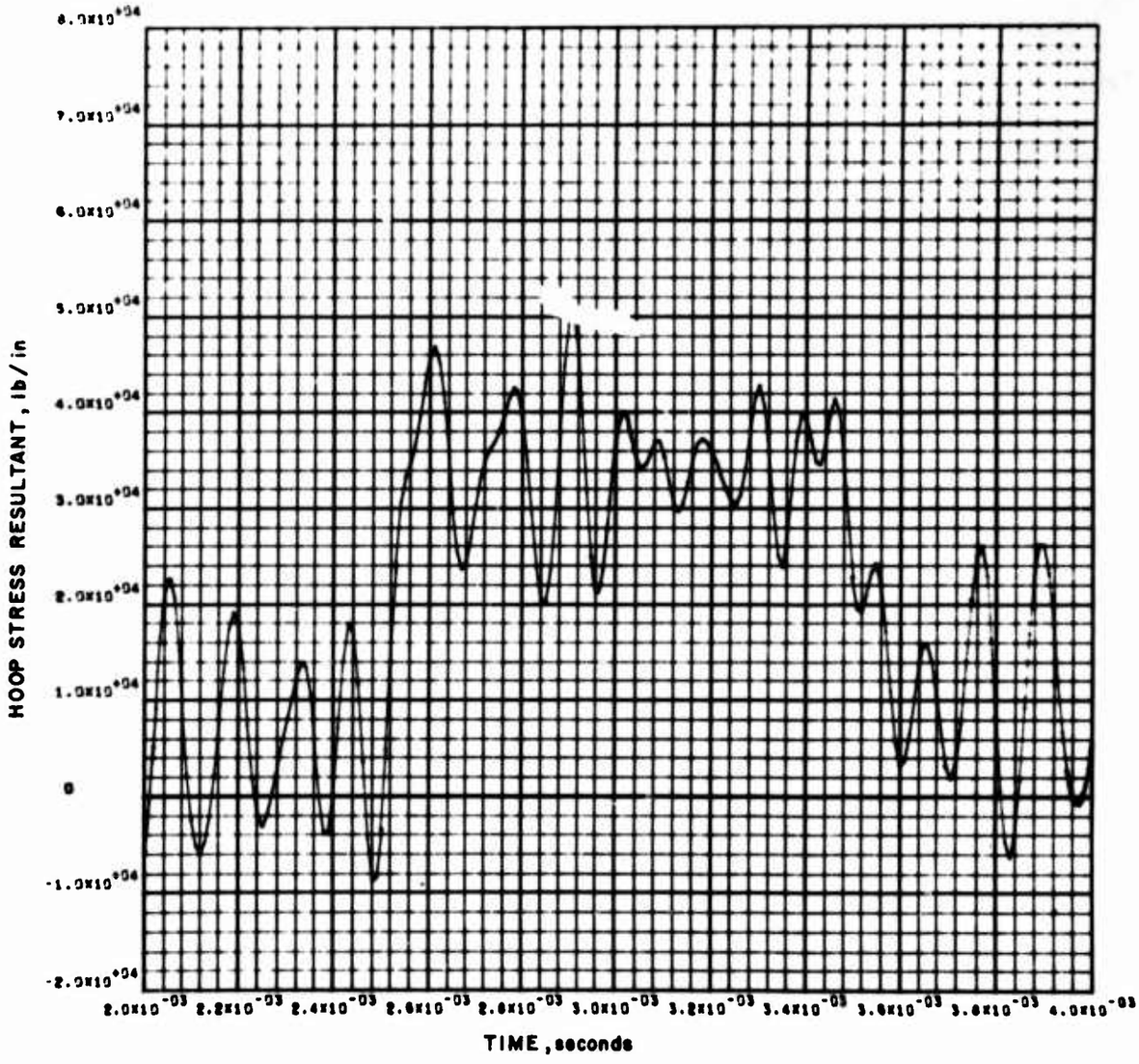

Figure 18 (Concl'd)

TABLE II. PEAK STRESS RESULTANTS--UNIFORM CYLINDER

Loading Condition	Peak Stress Resultant (lb/in)		von Mises Yield Function, J (lb/in)
	Axial	Hoop	
1 Longitudinal force only	-130,000	+25,000	
2 Radial pressure only	- 5,000	+82,000	
	Σ = -135,000	Σ = +107,000	211,000
3 Combined loading, including phasing	-130,000	+ 84,000	186,000

Values at midpoint of cylinder

TABLE III. COMP B EXPLOSIVE--MECHANICAL PROPERTIES

$$\delta = (B\rho)^{1/2} V$$

wax (percent)	B (lb/in^2)	ρ (lb/in^3)	$B\rho$	$(B\rho)^{1/2}$	$(B\rho)^{1/2}$ (ratio)	C (in/sec)
1	0.734×10^6	0.0624	0.0460×10^6	215	1.13	67500
2	0.512×10^6	0.0617	0.0316×10^6	177	0.94	56800
3	0.336×10^6	0.0610	0.0206×10^6	144	0.76	46100
Our case	0.578×10^6	0.062	0.0359×10^6	190	1.0	60000

The hoop stress resultants shown in Figure 18 for the radial pressure loading are substantially lower than in the uniform cylinder analysis. The maximum value is a tensile 54000 lb/in compared to 82000 for the uniform case. However, the shapes of the response curves are very similar.

The peak is lower for the tapered case, not because the thickness at the midpoint is 0.875 inch (versus 0.803 inch for the uniform case), but because the thicker front end more or less retards the magnitude of the oscillations about a mean value. Comparing Figures 12 and 18, it can be seen that both cases have essentially identical mean values of compressive hoop stress resultants in the period of 0.6 to 1.5 milliseconds. The difference in the peak values is that

the tapered case does not have as large oscillations about this mean value as does the uniform case.

The peak stress resultants for the tapered case have been compiled in Table IV. By combining the maximum values of the two loading conditions, the von Mises yield function is 22 percent greater than the analysis where phasing is accounted for. This indicates that by shifting the peak value to coincide at a given time, the total stress condition increases by 22 percent. This would be the effect of a possible change in filler material properties. As was the case in the uniform cylinder study, the radial pressure induces negligible axial stresses but causes large hoop stresses.

The maximum axial and hoop stresses due to the radial pressure load are presented in Figure 19 along the length of the cylinder. Both the uniform case and the tapered case are shown. For both cases, the radial pressure has a value of 9250 lb/in^2 at the impact end, and gradually decreases because of damping at the pressure wave front as it travels down the length of the cylinder.

Because the ends are restrained from expanding radially, the hoop stresses are zero at the ends. Also shown in the figure are the pseudo-static hoop stresses along the cylinder. These are the stresses which would occur at a given location if the pressure were statically applied to a ring having the radius and thickness at that given location. In the uniform cylinder, the dynamic load factor (peak load divided by pseudo-static load) is of the order of 1.7 along the length of the cylinder. For the tapered cylinder, the dynamic load factor ranges from 1.5 near the front end, down to 1.2 near the center and then up to 2.0 near the rear end. Generally, the dynamic load factor is less for the tapered cylinder in the front half of the shell because it has thicker walls there; conversely, where the walls become thinner, the dynamic load factor becomes greater than in the uniform case. Section V discusses the dynamic loading effect in greater detail.

As shown in Figure 19, the peak hoop stresses are considerably higher than the pseudo-static values. In general, the thinner the shell the higher the dynamic response of the shell to a suddenly applied radial pressure load.

For a step axial load such as was considered in this study, there is no advantage to a tapered shell because the stresses at the rear end are as great as at the front end for a uniform cylinder, and they are greater at the rear end for a tapered shell. This is because of the increasingly thinner walls going aft from the impact surface which results in increasing stresses. However, for bombs having nose shapes other than blunt-ended, the axial force builds up as a ramp function and peak stresses will be higher near the impact end. In this loading situation, the tapered shell will be more efficient than a uniform shell.

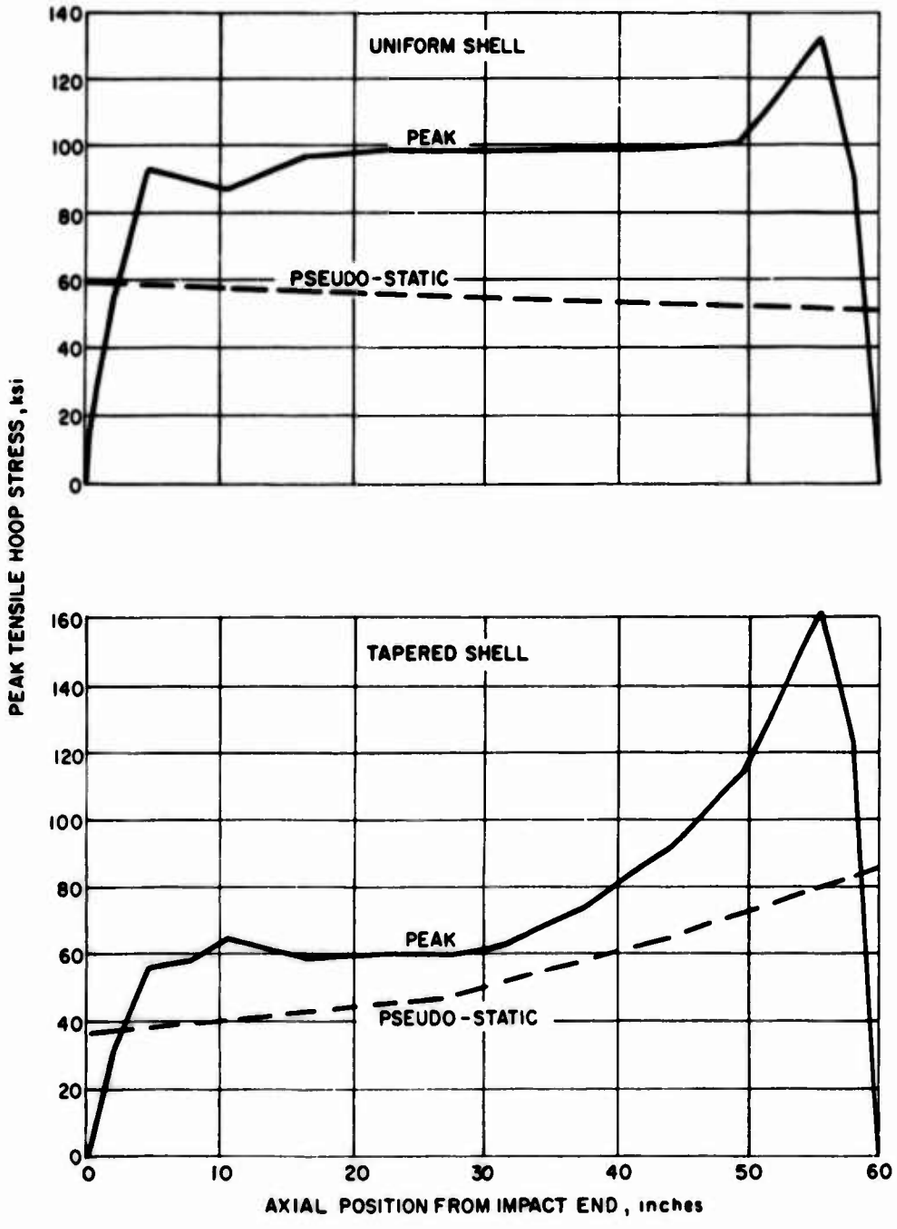

Figure 19 Peak Hoop Stresses Along Cylinder Length

TABLE IV. PEAK STRESS RESULTANTS -- TAPERED CYLINDER

Loading Condition	Peak Stress Resultant (lb/in)		J, lb/in von Mises Yield Function
	Axial	Hoop	
1 Longitudinal force only	-107,000	+20,000	
2 Radial pressure only	- 4,500	+54,000	
	Σ = -111,500	Σ = +74,000	162,000
3 Combined load, including phasing	-105,000	+44,000	133,000

Values at midpoint of cylinder

SECTION V

FURTHER ANALYTICAL STUDIES

Various analytical studies were conducted to obtain a general background of information on the impact response of filled shells. The results of these studies give a broad understanding of the types of effects which occur, a first-cut knowledge of the parameters controlling stress development and a set of concepts for interpreting the computer results which have been obtained. Some indication of aspects which require further study have also been deduced from the analytical investigations.

The following aspects of the impact of filled shells are of interest, for purely normal impact:

1) behavior of axial compression waves in the filler and shell due to sudden contact with the rigid target, and

2) radial response of the shell and filler due to Poisson coupling of axial stresses.

It will be seen that although the initial stresses produced by the impact are axial, the radial stresses which are coupled to the axial stresses through Poisson effects are highly significant as a source of failure in the shell.

In the actual response of the shell, the radial response modes are quite complicated because of axial bending and shear effects which couple the motion of adjacent sections. By ignoring this coupling along the axial direction, the radial response can be treated by the relatively simple approach considered later in this section. The more accurate analysis embodied in the computer results is required to account for the axial coupling effects.

A. AXIAL WAVE MOTION

The response of the filled shell under normal impact is governed in the first instance by axial compression waves which are propagated into the shell and filler. In either component the speed of the compression wave is given by

$$C = \sqrt{\frac{\lambda + 2\mu}{\rho}} \quad (\text{in-sec}^{-1})$$

where

μ = shear modulus, psi

λ = Lame's constant, psi

ρ = density, lb sec^2/in^4

It is convenient to express these constants in terms of engineering quantities, E (Young's modulus) and ν (Poisson's ratio). We get

$$\lambda + 2\mu = \left(\frac{1-\nu}{1+\nu}\right)\frac{E}{1-2\nu} \tag{4}$$

We note also that the bulk modulus, K, is given by

$$K = \frac{1}{3}\,\frac{E}{1-2\nu} \tag{5}$$

Then as ν approaches 0.5, corresponding to a fluid-like material, it is found by comparing Equations (4) and (5) that $\lambda + 2\mu \cong K$. For typical fillers, one expects $\nu \cong 0.45$, which gives

$$\lambda + 2\mu \cong 1.13K$$

$$\cong 3.33E$$

On the other hand for a typical metal, $\nu = 0.3$ and Equation (4) gives

$$\lambda + 2\mu \cong 1.345E$$

For the filler, the wave speed is approximately the square root of bulk modulus divided by density, while for the metal shell the wave speed is approximately the square root of Young's modulus divided by density.

For many fluids and fluid-like materials the wave speed is on the order of 60,000 in/sec, while for metals the speed is on the order of 200,000 in/sec. For a steel shell and a comp B filler with about 1.5 percent wax, the calculated values of wave speed are very close to the above values. These values were previously discussed in Section IV, paragraph A.

Figure 20 indicates that for impact with a perfectly rigid target, step pressure waves are propagated in the shell and filler starting at the contact point and moving toward the back end at the wave speed of each component. For a deforming target such a pressure step may still be generated, but the height of the step will be lower. For example, if the projectile hits a rigid target the velocity at the interface becomes zero and the axial pressure is given by

$$\sigma_A = \rho c\, V_o$$

where V_o is the impact velocity. For a projectile colliding with a body having similar deformation characteristics (i.e., for two identical bodies colliding) the interface velocity will be 0.5 V_o and

$$\sigma_A = \frac{1}{2}\,\rho c\, V_o$$

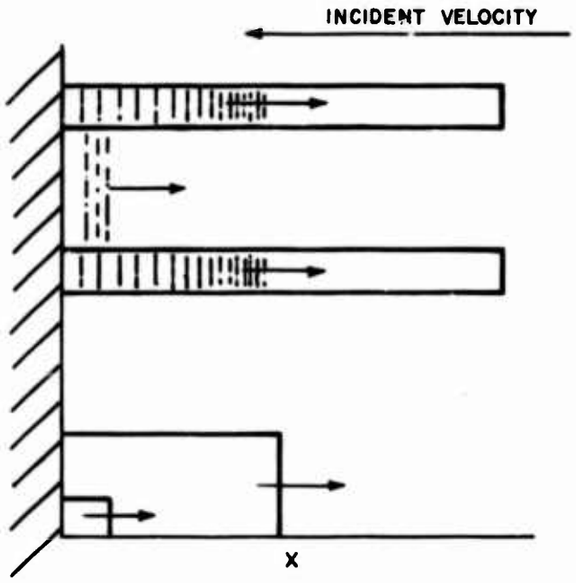

Figure 20 Compression Waves in Filled Shell

In these two cases the pressure at the interface remains constant until a reflected wave is returned from the back end. For impact with a large target which undergoes failure or other deformation modes, the force may be lower and will vary with time. At the instant of impact it is given approximately by

$$\sigma_A = \frac{\rho_t C_t}{\rho C} (\rho C V_o)$$

where ρ_t and C_t are the target density and sound speed.

For a concrete target, $C \cong 100{,}000$ in/sec (i.e., about half that of steel), while the density is about 0.33 times that of steel, whence $\rho_t C_t / \rho C = 1/6$ and

$$\sigma_A \cong \frac{1}{6} (\rho C V_o)$$

prior to target failure. After failure, the contact stress will drop to a value determined by the penetration characteristics of the projectile.

For steel, $\rho C = 140$ lb sec/in^3 whence for $V_o = 1000$ in/sec, $\rho C V_o$ is on the order of 140,000 psi so that the initial stress for the concrete target would be about 23,000 psi. The stress would proba. irop toward the bearing strength of the target in a few fractions of a microsecond. For the filler, it is found that

$$\rho_\delta C_\delta = 9.5 \text{ lb sec/in}^3$$

whence $\rho_\delta C_\delta V_o$ is about 9500 psi for V_o = 1000 in/sec. In the computer solutions discussed in Section IV, paragraph B, filler and shell stresses have been assumed corresponding to V_o close to 1000 in/sec; for real targets this implies that the actual projectile velocity was considerably higher, but due to target deformation characteristics the stresses developed correspond to approaching a rigid target at a reduced velocity.

An important effect on the overall projectile response may be produced by the end cap of the shell, especially at the back end. Figure 21 indicates the cases of interest. The behavior here may refer to either the shell or the filler. The figure at the top shows the step compression wave on its initial pass approaching the back end of the shell. When the step reaches the back end the subsequent response will depend on whether a large or small mass is attached to the end in the form of the end cap. For zero end mass (Figure 21B) a free surface reflection occurs which propagates a step of zero stress toward the front end. For an infinite mass (Figure 21C) a returning step of increased pressure amounting to twice the initial step is generated. For a finite end mass the situation is intermediate between these two situations (Figure 21D). Here the returning wave has an initial peak of $2\sigma_o$ corresponding to the infinite mass, but it decays to zero exponentially, thus agreeing with the zero mass end condition. The exponential decay is an approximation which is obtained on assuming that the back plate acts as a rigid lumped mass, thus ignoring possible bending effects in the plate.

The exponential drop-off can be shown to be given by

$$\sigma_e = 2(\rho C V_o)\, e^{-t/\tau} \qquad (6)$$

where

$$\tau = \frac{t_e}{t_s}\,\frac{R}{2C}$$

Here

R = shell radius, in

C = wave speed in the shell, in/sec

t_e = thickness of the end plate

t_s = wall thickness of the shell

Note that the stress σ_e in Equation (6) represents the variation of stress with time at a fixed position along the shell. Likewise, as the returning peak of $2\sigma_o$ moves toward the front end at a velocity C, the exponential drop off is distributed along the shell as indicated in Figure 21D.

The level therefore decays by a factor of 1/e in a distance $\bar{X}$ where

$$\bar{X} = C\tau = \frac{t_e}{t_s}\,\frac{R}{2} \qquad (7)$$

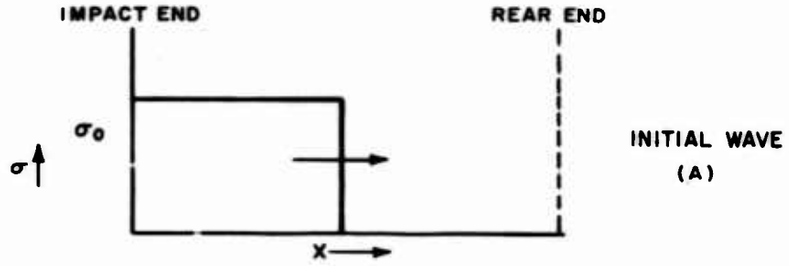

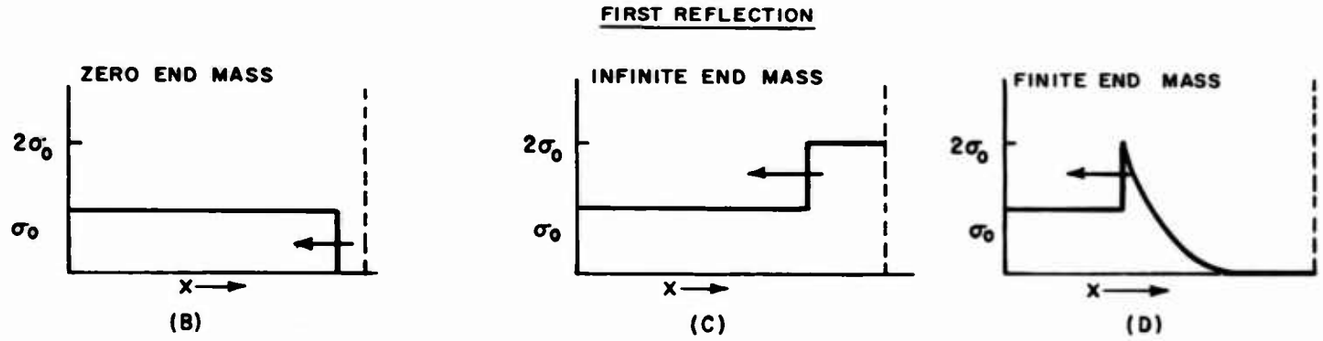

Figure 21 Effect of End Mass

If the end plate is the same order of thickness as the shell wall ($t_e \cong t_s$) the stress drops by $1/e$ in an axial distance equal to half the radius.

In computer solutions to date, the end mass effect has been ignored to avoid undue complication of initial results. The available computer program can accommodate this type of end condition however, and a matter of apparent future interest is the investigation of the modification of results produced by the end mass. The $2\sigma_o$ returning peak could significantly aggravate the tendency toward shell failure, although its effect may be reduced if the decay time τ is sufficiently short.

In the case of the filler, the effect of the end plate will depend on whether the shell is filled completely to provide contact between the filler and back plate. For a partially filled shell with a gap at the rear end the free surface (zero mass) reflection conditions will occur.

Axial stress predictions obtained from the one-dimensional theory are shown in Figure 22. These include: 1) the axial stress in the shell (solid curves) as a function of time at various stations along the shell; and 2) pressure in the filler (dashed curve) as a function of time. The loading as well as the shell and filler parameters are the same as those assumed in Section IV, paragraphs A and B.

Figure 23 gives a comparison of the simple theory prediction of shell stress with the computer results given in Figure 9 for $x = L/2$. Differences between the two results are at least partly associated with the more complete model used for the computer prediction. The higher frequency oscillation in the computer results are probably a result of coupling of radial motion. The computer results may be somewhat affected by the number of modes assumed; a larger number of modes may be required to obtain complete accuracy in simulating the abrupt changes of slope predicted by the one-dimensional model.

B. RADIAL RESPONSE

If the radial deformation of the shell and filler could be ignored, the shell response for a uniform thickness could be treated exactly by the one-dimensional theory discussed in the previous section. However, significant effects are produced by radial deformation due to Poisson coupling between axial and radial motion. For example, the axial compression wave in the shell tends to produce a radial expansion related to the initial axial strain, ϵ_o, times the Poissons ratio of the shell, ν_s. Under static loading condition the hoop strain in the shell, ϵ_{hs}, would be

$$\epsilon_{hs} = \nu_s \epsilon_o = \frac{w}{R}$$

where w = radial deformation, while the hoop stress would be zero. In the dynamic case of a suddenly developed axial stress, we can approximate the response by noting that the shell will tend to expand radially by the amount

$$\bar{w} = \nu_s \epsilon_o R \qquad (8)$$

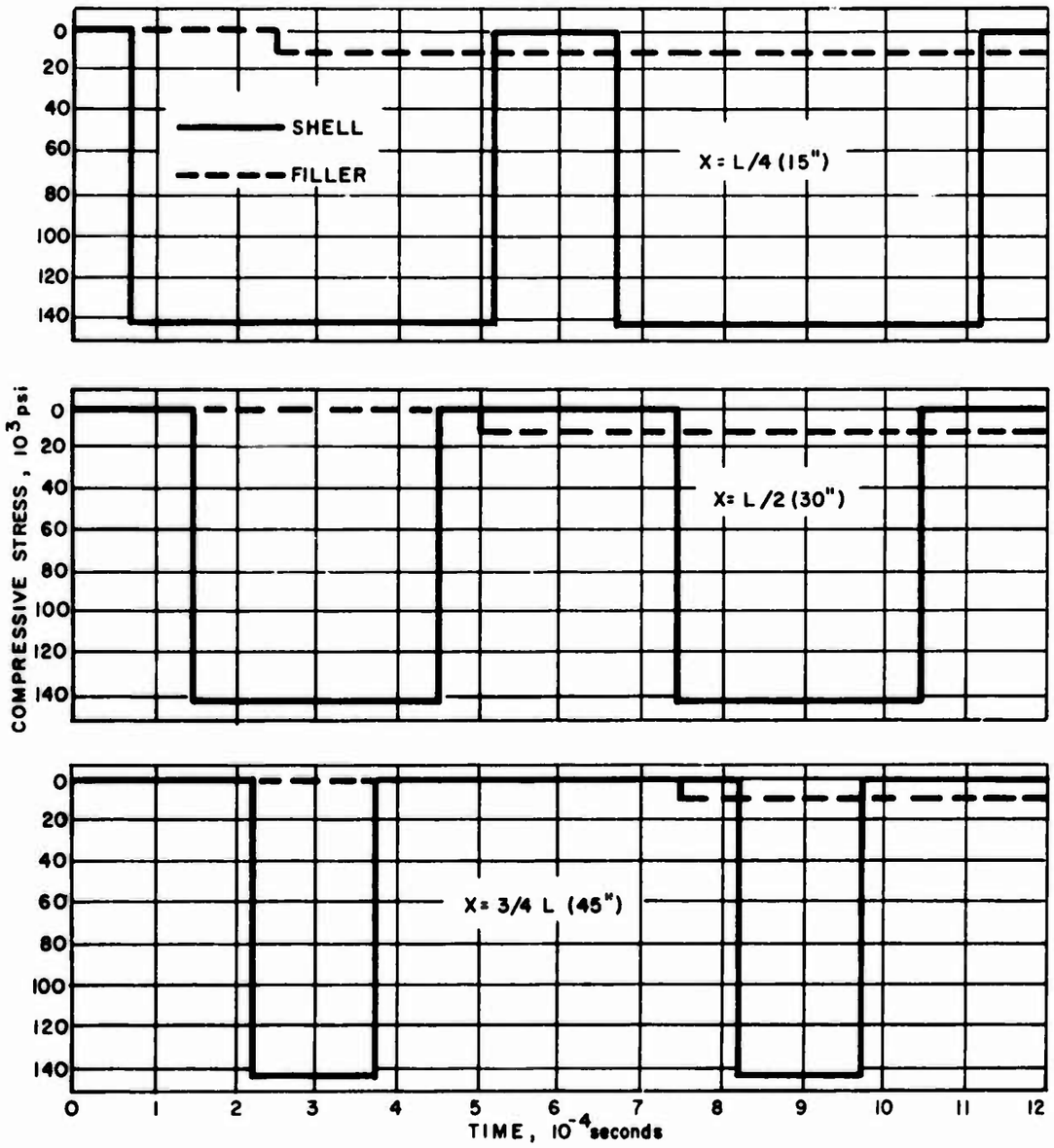

Figure 22 Axial Stress Predictions by One-Dimensional Theory
(Zero End Mass Condition)

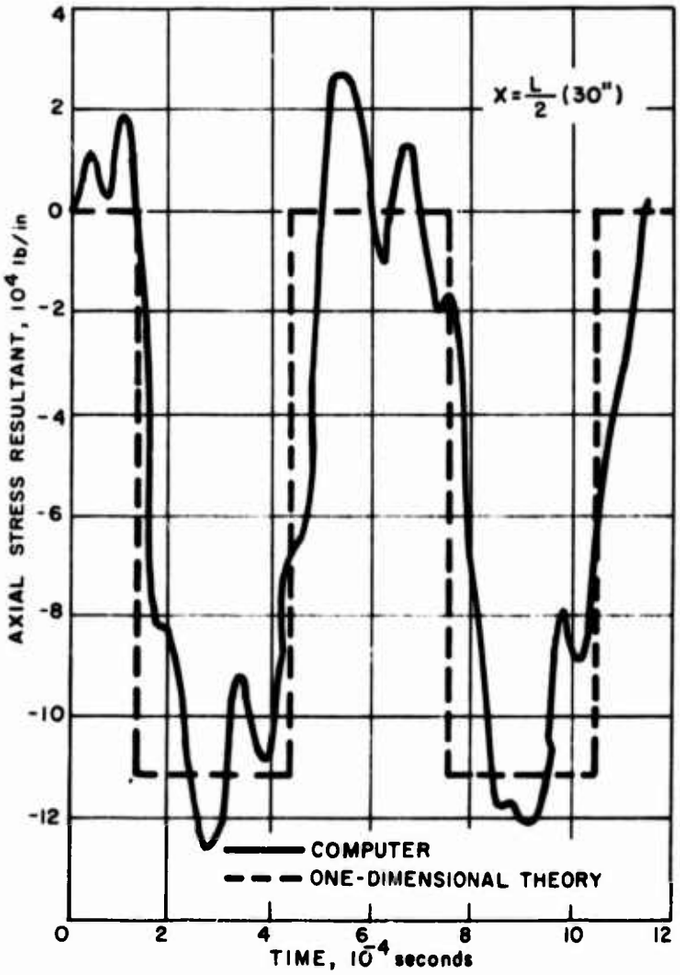

Figure 23 Comparison of One-Dimensional Solution with Computer Results

but will be prevented by the inertia of the shell from reaching this deflection instantaneously. An initial compressive stress of $E\varepsilon_s$ is therefore generated. Furthermore, the shell will overshoot the static deflection point because of kinetic energy which is built up, and sections of the shell tend to oscillate radially after the first axial compression wave has passed, at a period approximately equal to the "breathing mode" period of the shell, in which each section expands and contracts as a ring. For sufficiently long shells, the breathing mode frequency is given by

$$f_b = \frac{C}{2\pi R} \tag{9}$$

so that the period of this oscillation is

$$\tau_b = \frac{2\pi R}{C} \tag{10}$$

For C = 200,000 in/sec and R = 5.625 inches we get f_b = 5660 cps which is approximately the frequency of mode 5 given in Table I. This oscillation begins at a given point with the passage of the axial pressure step.

This picture must be modified by taking shear coupling between adjacent sections of the shell into account, as is done in the computer solutions which have been obtained. Shear effects in the shell will tend to retard the complete development of the radial expansion because of coupling between disturbed and undisturbed sections of the shell. Ignoring this coupling effect gives an upper bound estimate of the radial expansion which can be expected. We note first of all that the axial strain, ϵ_o, in the shell is given by

$$\epsilon_o = \frac{V_o}{C} \tag{11}$$

for the step stress assumed at the front of the shell. Then the value of deformation given by Equation (4) is

$$\bar{w} = \nu_s \frac{V_o}{C} R \tag{12}$$

which is the value of w for static loading. For the case of sudden loading, the final value of w will be twice $\bar{w}$ due to inertial overshoot. (The factor of 2 corresponds to the response of a spring-mass system in which a force is suddenly applied to the mass and held constant.) As a result, in the case of the filled shell, a hoop stress σ_h given by

$$\sigma_h = E \frac{\bar{w}}{R} = \nu_s \sigma_A \tag{13}$$

tends to occur.

This stress is associated only with the first axial wave in the shell.

Additional radial deformation is generated by the pressure wave in the filler, although this occurs at a later time. The radial pressure exerted by the filler is approximately equal to the axial pressure because of the fluid-like response of the filler. (The actual radial pressure is given by

$$\sigma_{rf} = \frac{\nu}{1-\nu} \sigma_{Af} \tag{14}$$

where

$$\sigma_{Af} = \rho_f C_f V_o \tag{15}$$

is the axial pressure in the filler and σ_{rf} is the radial pressure. For ν_f = 0.45, we have $\sigma_{rf} = 0.82\ \sigma_{Af}$.)

This radial pressure is exerted against the shell and will tend to produce a static hoop stress,

$$\sigma_{hs} = \frac{R}{t_s} \sigma_{rf}$$

in the shell. Again however, due to the dynamic aspects of the shell response an inertial overshoot will occur and will produce a maximum stress equal to twice this value. Therefore a simple estimate for the hoop stress in the shell due to radial pressure in the filler is

$$\sigma_{hs} = \frac{2R}{t_s} \sigma_{rf} \tag{16}$$

It is of interest to compare the radial stresses predicted by the simple formulas, Equations (13) and (16), with the maximum values obtained by the computer evaluations (see Section IV, paragraph B). The case of interest is the uniform thickness shell with a step pressure loading given by σ_{AS} = 144,000 psi in the shell and σ_{Af} = 9250 psi in the filler, corresponding to V_o = 960 in/sec. The shell parameters of interest are

$$\nu_s = 0.3, \quad t_s = 0.8 \text{ inch}, \quad R = 5.625 \text{ inches}$$

Note that the simplified predictions given here serve as bounds on the values expected from the more accurate computer runs, since the radial response should be greater than the static prediction because of inertial overshoot but less than the dynamic prediction because of shear coupling effects in the shell. Then the following comparisons are obtained between the simple formulas and the computer runs:

Induced Hoop Stress in Shell

	Stress Due to Poisson Effect in Shell Alone (psi)	Due to Filler Radial Pressure (psi)
Static Prediction	0	65,000
Dynamic Prediction	43,150	130,000
Computer Prediction	31,000	102,500
Ratio, Computer/Dynamic	0.72	0.78

These results indicate that the actual radial response for a step pressure wave is 20 to 30 percent less than the dynamic prediction based on the simplified ring response model.

The type of predictions of hoop stress based on the simplified theory are shown in Figure 24. These may be compared with the computer results shown in Figures 11 and 12 which show the separate effect of axial load in the shell and radial pressure exerted by the filler. Figure 24, for the simple theory, shows the

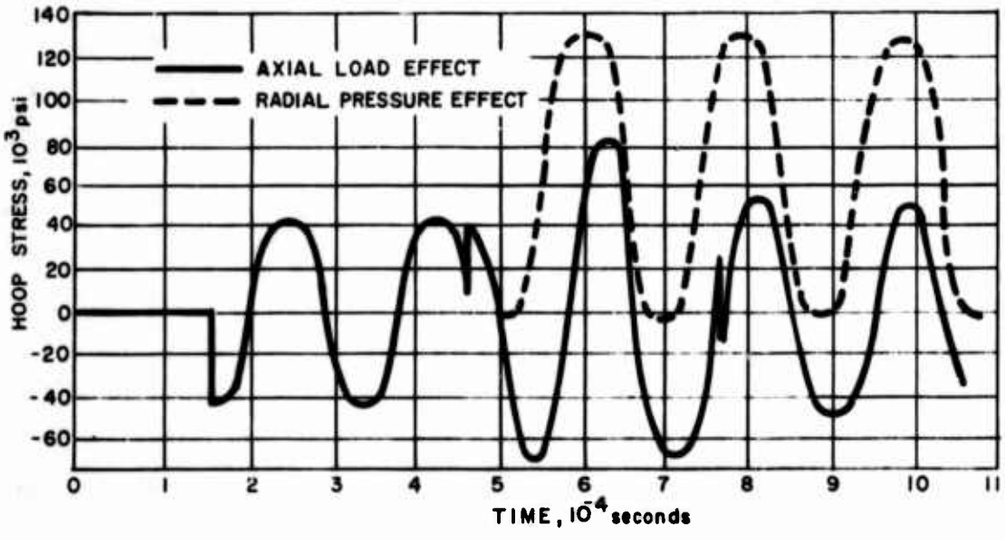

HOOP STRESS IN SHELL

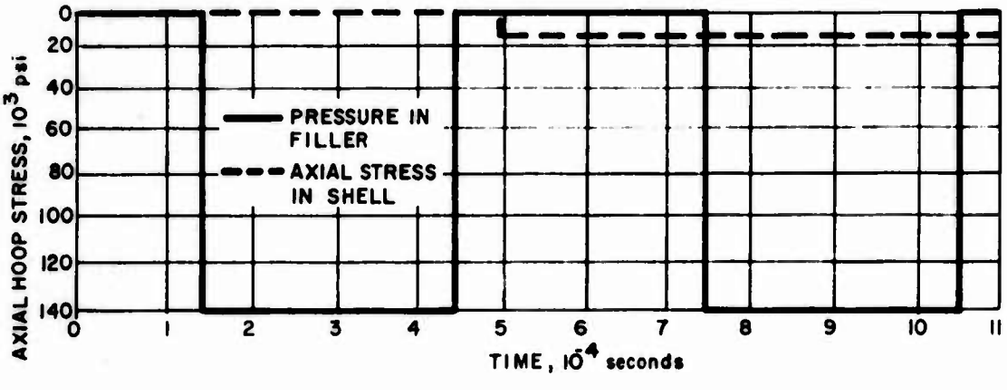

AXIAL STRESSES IN SHELL AND FILLER

Figure 24 Simplified Predictions of Shell Hoop Stress, x = L/2 (30 inches)

response for both types of loading. As with the comparisons of computer and simplified analyses for axial motion, the results are on the same order of magnitude for the two predictions, but differences occur because of the incomplete model used for the simplified theory and the suppression of high order modes in the computer solution. Detailed comparisons of hoop stress time traces are particularly difficult because minor differences in the phasing of various components will cause large changes in the detailed appearance of the resultant trace.

One point of interest in the combined response prediction is the possibility of resonance between the axial and radial motion.

The ratio of radial-to-axial period is given approximately by $2\pi R/L$, and for certain values of this ratio, the passage of the axial wave may continuously reinforce the radial motion over several axial periods. This type of resonant reinforcement should be studied further to determine whether it might aggravate failure for particular classes of shell design.

SECTION VI

CONCLUSIONS

Cylinders of both uniform thickness and linearly varying thickness have been studied to determine the effect of the filler material on the structural integrity of the shell. The loading condition considered was a longitudinal impact of the combined shell-filler system with a concrete target which fails and allows penetration by the shell.

In the analysis, the bonding between the filler material and the shell interior wall has been ignored. The filler material acts as a liquid which exerts a radial pressure on the shell walls during the impact and penetration event. Since the filler does not modify or restrain the axial motion of the shell in the assumed analytic model it contributes negligibly to the axial stresses in the shell. However, it induces a significant hoop stress in the shell.

Since the analytic solution applies to a linear elastic system, results are directly proportional to the forcing input and may be ratioed by any desired factor to account for faster or slower impact conditions. For example, the results plotted in all of the figures and tables in this report are applicable for a 1000 ft/sec impact velocity into a concrete target and for an assumed axial force which has been estimated on the basis of past experience and experimental data. For other impact velocities and target materials this axial force would change in magnitude. More important, the referenced estimates of the axial load may be revised as more experimental data and evidence become available. Revised stress results can be obtained by a direct ratio of the revised force to the force used in this report.

More investigation is required as to the mode and sequence of failure of the target upon impact. With concrete, a given stress level must be reached before the target surface will yield and allow penetration. With a blunt-end, there will be an instant when this end is stopped completely from its impact velocity. Only after the target surface has failed will this front end begin to penetrate. For the uniform cylinder studied here, the initial particle velocity was of the order of 970 in/sec, far lower than the impact velocity of 12,000 in/sec. The 970 value was obtained from the Poncelet force expression relationship and solving for particle velocity from Equation (3) of Section IV. Actually, the front end of the cylinder would feel a velocity change of 12,000 in/sec for a very short time and then a much lower velocity after the target has given way. In this study the pulse caused by the target before failure was ignored.

Hoop stresses are a substantial part of the total stress acting at a given point. In fact, many bomb case failures occur as longitudinal cracks running for substantial lengths along the cylindrical shell. This type of failure can be caused by large tensile hoop stresses induced by the filler material within the shell walls. For the shell designs considered in this report, hoop stresses of the order of 104,000 to 134,000 psi are predicted at impact velocity of 1000 ft/sec for the uniform cylinder. Values up to 162,000 psi (near the rear end) are found in the tapered configuration. These are large stresses and do form a large part of the total stress condition in the bomb casing. Table V presents the radial pressure loading peak hoop stresses predicted for these bomb configurations for impacts of 1000, 1500, and 2000 ft/sec.

The values given in the table range from 134,000 to 162,000 psi for the uniform and tapered cases, respectively, at an impact velocity of 1000 ft/sec. This impact velocity is certainly a reasonable expectation of present bombs. For a 2000 ft/sec impact, stresses are in excess of 300,000 psi. With bomb structures manufactured from steels having yield strengths as low as 75,000 psi, the possibility of hoop stress failures is great. Even high strength steels with yield strengths around 300,000 psi would be susceptible to cracking. In addition, cutouts or other discontinuities in the shell structure which introduce stress concentrations would greatly aggrevate the situation.

It should be recalled that the values given in the table apply to a filler material having a bulk modulus (B) of 0.578×10^6 psi and a density (ρ) of 0.062 lb/in^3. Hoop stresses due to radial pressure may be found for other materials by applying the relation

$$\delta_x = \delta_H \left[\frac{(B\rho)_x}{(B\rho)_H}\right]^{1/2}$$

where

δ_x = hoop stress of filler material x

δ_H = hoop stress of filler material used in this report

$(B\rho)_x$ = properties of filler material x

$(B\rho)_H$ = properties of filler material used in this report

TABLE V. PEAK HOOP STRESS AS A FUNCTION OF IMPACT VELOCITY

Impact Velocity (ft/sec)	Peak Hoop Stress (psi)	
	Uniform Shell	Tapered Shell
1000	134,000	162,000
2000	303,000	369,000
3000	537,000	650,000

Loading Condition-Radial Pressure Induced by Filler

In examining the results of this study, it has become apparent that the bonding between the filler and the shell wall can play an important part in evaluating shell stresses. This bonding effect would influence both axial and hoop stresses. Since no axial shear is present in the models studied, the filler and the shell oscillate longitudinally, completely independent of each other. This is also true in the radial direction, where the shell radial oscillations are presently assumed to be unaffected by the filler and the bond.

In conjunction with the bonding effects, damping properties of the filler would enter strongly into shell stresses. The present analysis somewhat arbitrarily assumes 5 percent structural damping in the filler. It is suspected that this value may be low by a factor of two or more. If true, it would combine with the bonding effect to possibly produce significant changes in both hoop and axial stresses.

Another point brought out by the analysis is that these stresses apply only to a blunt-ended cylinder. As such, the axial loading is a step function and results in very high stresses throughout the cylinder as reported in this study. A bomb designed to attack a concrete target would probably have a conical or ogival nose shape. It would then experience a ramp-type of forcing function, with resulting lower stresses throughout the cylinder because of the relatively more gradual application of the force.

In conclusion, this study has pointed out the effect of the filler material upon the structural loading of a bomb impacting a concrete target. The filler accounts for a major portion of the shell stresses. Modifications to this present study have come to light to determine a possibly more realistic evaluation of these effects. In particular, investigations of the shell-filler bonding effects and filler damping properties would improve the results obtained in the present study. Also of interest would be the determination of stresses for the more general penetrating bomb configurations which have conical or ogival noses as opposed to the blunt-ended cylinders studied in this report.

REFERENCES

1. Percy, J. H., D. R. Navaratna and S. Klein, SABOR III, A Fortran Program for the Linear Elastic Analysis of Thin Shells of Revolution under Axisymmetric or Asymmetric Loading by Using the Matrix Displacement Method, MIT ASRL TR 121-6 (May 1965).

2. An Analytical Study of a New Reentry Vehicle Weapon System, WL-TDR-64-99, Final Report, Avco/RAD (August 1965). Secret R/D

3. Terradynamic Loading and Vehicle Response Program, Final Report, Avco/SSD (January 1969). Secret

4. 175-mm Concrete Penetrating Projectile Program (U), Phase II - Design Study Report, AVSSD-0363-66-RR, Final Report, Avco/SSD (December 1966). Confidential

5. Mooney, D. T., and R. H. Coco, The Evaluation of Lumped Mass Techniques for Solving Stress Wave Propagation, Avco Internal Memorandum, TR S310-T-150 (12 May 1965).

6. Timoshenko, S., and J. Goodier, Theory of Elasticity, 2nd Edition, McGraw-Hill Book Company (1951).

7. Love, A. E. H., A Treatise on the Mathematical Theory of Elasticity, 4th Edition, Dover Publications.

(The reverse of this page is blank)

UNCLASSIFIED

Security Classification

DOCUMENT CONTROL DATA - R & D

(Security classification of title, body of abstract and indexing annotation must be entered when the overall report is classified)

1. ORIGINATING ACTIVITY (Corporate author) Avco Government Products Group Space Systems Division Lowell, Massachusetts	2a. REPORT SECURITY CLASSIFICATION Unclassified 2b. GROUP

3. REPORT TITLE

EFFECTS OF FILLER MATERIAL ON BOMB FRACTURE

4. DESCRIPTIVE NOTES (Type of report and inclusive dates)
Final Report - 13 June 1968 to 12 January 1969

5. AUTHOR(S) (First name, middle initial, last name)

M. H. Miller
R. W. Johnson

6. REPORT DATE	7a. TOTAL NO. OF PAGES	7b. NO. OF REFS
February 1969	71	7

8a. CONTRACT OR GRANT NO.	9a. ORIGINATOR'S REPORT NUMBER(S)
F08635-68-C-0129 b. PROJECT NO.	AVSSD-0008-69-RR
c. d.	9b. OTHER REPORT NO(S) (Any other numbers that may be assigned this report) AFATL-TR-69-14

10. DISTRIBUTION STATEMENT
This document is subject to special export controls and each transmittal to foreign governments or foreign nationals may be made only with prior approval of the Air Force Armament Laboratory (ATRW), Eglin AFB, Florida 32542.

11. SUPPLEMENTARY NOTES	12. SPONSORING MILITARY ACTIVITY
Available in DDC	Air Force Armament Laboratory Air Force Systems Command Eglin Air Force Base, Florida 32542

13. ABSTRACT

Avco Corporation, Space Systems Division, has completed a six month analytical program which investigated the effects of the explosive filler material on the structural failure of bomb casings during impact and penetration into hard targets.

A typical cylindrical shell, similar to the present BLU-31B bomb was studied. Both constant and linearly varying wall thicknesses were investigated. To obtain a basic understanding of the filler effect, only an axial load, suddenly applied and held constant, was included. A finite element solution was used to obtain resulting stresses and displacements within the casing. Results indicate the large effect of the filler on the hoop stresses. These stresses are of sufficient magnitude to induce casing failure based on current bomb designs and impacting conditions against concrete targets.

Results are presented for a typical Composition B explosive filler material. Hoop stress magnitudes may be obtained for any other filler material, using given relationships between its bulk modulus and density properties compared to the Composition B properties.

DD FORM 1 NOV 68 1473

UNCLASSIFIED

Security Classification

14 KEY WORDS	LINK A		LINK B		LINK C	
	ROLE	WT	ROLE	WT	ROLE	WT
Filler Material						
Structural Integrity						
Bomb Fracture						
Target Defeat Mechanism						
Explosive Capability						